Mr Bowman D-2

for attribution

Duplicate

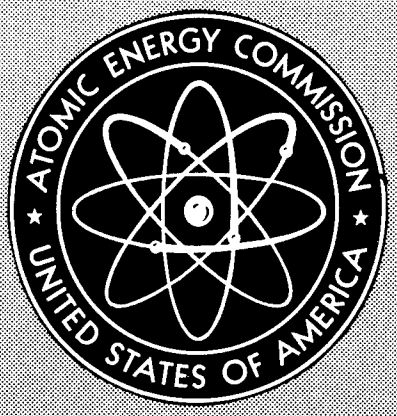

TID-13485

HEAT TRANSFER AND PRESSURE DROP FOR A GAS AT HIGH TEMPERATURE

Technical Report

By
Monty E. Davenport
Patrick M. Magee
George Leppert

May 1961

Nuclear Technology Laboratory
Stanford University
Stanford, California

UNITED STATES ATOMIC ENERGY COMMISSION • DIVISION OF TECHNICAL INFORMATION

Other issues of this report may bear the No. SU-247-2.

LEGAL NOTICE

This report has been reproduced directly from the best available copy.

Printed in USA. Price $1.50. Available from the Office of Technical Services, Department of Commerce, Washington 25, D. C.

USAEC Division of Technical Information Extension, Oak Ridge, Tennessee

TID-13485

ENGINEERING AND EQUIPMENT

HEAT TRANSFER AND PRESSURE DROP FOR A GAS AT HIGH TEMPERATURE

Technical Report 247-2

by

Monty E. Davenport
Patrick M. Magee
George Leppert, Principal Investigator

Submitted to

Division of Reactor Development
United States Atomic Energy Commission

May 1961

Contract No. AT(04-3)-247

Nuclear Technology Laboratory
Department of Mechanical Engineering
Stanford University
Stanford, California

TABLE OF CONTENTS

LIST OF ILLUSTRATIONS

NOMENCLATURE

English Letter Symbols

A	surface area	sq ft
a	exponent	
C_p	specific heat at constant pressure	Btu/(lb)(^oF)
D	diameter	ft
F	Fahrenheit	
G	mass flow velocity, ρu	lb/(sq ft)(hr)
g_c	conversion factor, 4.17×10^8	(lb)(ft)/(lb_f)(hr^2)
H	enthalpy	Btu/lb
h	convective heat transfer coefficient	Btu/(hr)(sq ft)(^oF)
J	conversion factor, 778	(ft)(lb_f)/Btu
k	thermal conductivity	Btu/(hr)(ft)(^oF)
L	test section length	ft
P	absolute pressure	lb_f/sq ft
p	gage pressure	lb_f/sq ft
q	heat transfer rate	Btu/hr
q'	heat transfer rate per unit langth	Btu/(hr)(ft)
q"	heat flux	Btu/(hr)(sq ft)
q'''	heat generation per unit volume	Btu/(hr)(cu ft)
R	Rankine	
$\mathcal{R}$	recovery factor	
r	Radial coordinate	ft
T	temperature, ^oR	
t	temperature, ^oF	
u	bulk velocity of gas	ft/hr
w	flow rate	lb/hr
x	axial coordinate	ft

Subscripts (refers to)

a	axial
av	average
aw	adiabatic wall
b	evaluated at bulk temperature

e	entrance to test section	
f	evaluated at film temperature,	$T_f = 0.5(T_w-T_b)+T_b$
o	stagnation conditions	
wo	outside surface of test section tube	
r	radial	
T	total	
t	test section tube	
w	inside surface of test section tube	
0.4	evaluated at reference temperature,	$T_{0.4}=0.4(T_w-T_b)+T_b$

NOTE: The lack of a subscript on gas properties indicates bulk properties.

Greek Letter Symbols

β	heat flux parameter	$q_w'' \sqrt{\rho_w \tau_w}/C_p \tau_w T_w$
$\Delta( )$	change of	
μ	viscosity	lb/(hr)(ft)
ρ	density	lb/cu ft
τ	shear stress	lb_f/sq ft
$\phi( )$	function of	

Non-dimensional Parameters

N_{Nu}	Nusselt number	hD/k
N_{Pr}	Prandtl number	$\mu C_p/k$
N_{Re}	Reynolds number	$\rho uD/\mu$
$\frac{T_w}{T_b}$	temperature parameter	
$\frac{x}{D}$	axial position parameter	
f	friction factor	$\frac{\tau_w}{\frac{\rho u^2}{2g_c}}$

1. SUMMARY

A research program entitled "Heat Transfer to a Gas at High Temperature" is being conducted at the Stanford University Nuclear Technology Laboratory under contract with the United States Atomic Energy Commission, and this report presents the results of the second phase of that program. The results of the first phase are given in Technical Report No. 247-1 (2)*.

Local convective heat transfer coefficients and local and average friction factors were measured for nitrogen flowing through an electrically heated, smooth, round tube. Data are reported for a range of Reynolds numbers from 1800 to 90,000, surface temperatures to 1455°F, gas temperatures to 780°F, and heat fluxes to 138,000 Btu/(hr)(sq ft).

It was found that the local heat transfer data could be correlated by the equation,

$$N_{Nu} = 0.020(N_{Re})^{0.8}(N_{Pr})^{0.4}\left(\frac{T_w}{T_b}\right)^{-0.5}\left[1 + \left(\frac{x}{D}\right)^{-0.7}\right]$$

for Reynolds numbers above 10,000.

There was considerable variation in local friction factor along the test section; however, the values determined near the exit (but far enough from the exit to eliminate end effects) were correlated by the relation,

$$\frac{1}{\sqrt{4f_f}} = 2 \log (N_{Re,f}\sqrt{4f_f}) - 0.8$$

for Reynolds numbers above 10,000 with fluid properties evaluated at the average of the wall and the gas bulk temperature. Average friction factor data were also correlated by this equation for Reynolds numbers above 20,000 but with fluid properties evaluated at bulk temperature. At lower Reynolds numbers, the experimental friction factors fell considerably above these predicted by the equation.

*Number in parentheses refers to the number of the reference appearing in the List of References.

2. INTRODUCTION

2.1 DEFINITION OF HEAT TRANSFER COEFFICIENTS

In the analysis of convective heat transfer processes between surfaces and fluids, it is common practice to employ a convective heat transfer coefficient, h, to relate the heat flux between the surface and the fluid, q''_w, at a point, to the difference between the surface temperature, T_w, and a characteristic temperature of the fluid at that point. For incompressible pipe flow , the local heat transfer coefficient is ordinarily based on the mean stream temperature. For high-speed compressible flow, however, it is more appropriate to base h on the adiabatic wall temperature, T_{aw}, which is the temperature that an insulated tube wall would assume at the same Reynolds number and Prandtl number. With any other method of defining h, it would be possible for h to have both negative and positive values. Moreover, it has been shown (15) that the value of h defined in terms of $(T_w - T_{aw})$ is the only one leading to an experimental correlation which is independent of the rate of heat transfer. Accordingly, the local heat transfer coefficient is defined by the equation

$$q''_w = h\,(T_w - T_{aw}), \qquad 1$$

The adiabatic wall temperature is commonly expressed in terms of the recovery factor $\mathcal{R}$:

$$T_{aw} = T + \mathcal{R}\,(T_o - T) \qquad 2$$

Shapiro (15) indicates that, to a good approximation,

$$\mathcal{R} = N_{Pr}^{1/2} \qquad 3$$

for laminar flow and

$$\mathcal{R} = N_{Pr}^{1/3} \qquad 4$$

for turbulent flow. Thus for air the recovery factors for the laminar and turbulent boundary layers are approximately 0.85 and 0.90, respectively.

The use of a local heat transfer coefficient is perfectly clear. However, in those cases where primary interest is focused on the total heat transfer rate, and detailed temperature and heat flux distributions are of no particular concern, it has been found convenient to define average heat transfer coefficients (in contrast to local values as in equation 1) by

$$q''_{w,av} = h_{av}(T_{w,av} - T_{aw,av}) \qquad 1a$$

In the case of heat transfer processes for fluids flowing through circular tubes, the heat flux and temperature averages are properly calculated by dividing the integrated values along the heated, or cooled, section by the total length of the section.

2.2 DEFINITIONS OF FRICTION FACTORS

Pressure loss for internal flow of fluids through channels is most conveniently related to the flow parameters through the use of a friction factor. The local friction factor, f, may be defined as

$$f = \frac{\tau_w}{\frac{\rho u^2}{2g_c}} \qquad 5$$

Momentum considerations for the steady flow of fluids through circular tubes lead to the following expression for the apparent wall shear stress, τ_w, in terms of quantities which may be determined experimentally:

$$\tau_w = \frac{D}{4}\frac{d}{dx}\left\{P + \frac{\rho u^2}{g_c}\right\} \qquad 6$$

This expression, which neglects the change in elevation, assumes that the static pressure is uniform across the flow cross-section and neglects the effect of changing velocity profile shape on the momentum flux, $\frac{\rho u^2}{g_c}$. The pressure is measured by means of taps on the test section, while the acceleration term is computed using the bulk gas temperature and the known flow rate.

An average friction factor may be defined as

$$f_{av} = \frac{\tau_{w,av}}{\frac{\rho_{av}}{2g_c}(u_{av})^2} \qquad 7$$

or equivalently as

$$f_{av} = \frac{\tau_{w,av}}{\frac{G^2}{2\rho_{av} g_c}} \qquad 8$$

The average apparent wall shear stress, $\tau_{w,av}$, over a distance from station 1 to station 2 may be calculated from the equation,

$$\tau_{w,av} = \frac{D}{4x_{1-2}} \left\{ \left[P_2 - P_1 \right] + \left[\left(\frac{\rho u^2}{g_c} \right)_2 - \left(\frac{\rho u^2}{g_c} \right)_1 \right] \right\} \qquad 9$$

It is often useful for correlation purposes to define a "film" friction factor:

$$f_f = \frac{\tau_w}{\frac{\rho_f u^2}{2g_c}} \qquad 10$$

where ρ_f is the fluid density evaluated at some reference temperature as later discussed in Section 3.

3. RELEVANT CORRELATIONS AND TECHNIQUES

A number of empirical and semi-analytical methods for predicting heat transfer coefficients and friction factors have arisen from investigations of forced convection heating of gases flowing turbulently through circular tubes, and a brief review of the more common methods is given below. Particular attention is focused on those correlations which are pertinent to the case of high temperatures and large temperature differences between the surface and gas.

3.1 THERMAL ENTRANCE REGION*

Investigations (3,4,6,7,10,14,23) of convective heat transfer have shown that, in general, h is not constant along a tube but may vary markedly with x/D, especially near the tube entrance; h tends to decrease from a high value near the entrance and to approach a constant value for large values of x/D (14,23). The primary cause of this variation is that the temperature profile across the flow stream is not fully developed at the entrance of a heated section (even though the velocity profile may be developed at the entrance). Consequently, as the temperature profile becomes developed downstream from the entrance, the heat transfer coefficient approaches an asymptotic value. Although the effect is not as pronounced in the case of turbulent flow as in the case of laminar flow, it is plainly evident from existing experimental results (14).

The variation of the heat transfer coefficient or, alternately, of the Nusselt number in the entrance region depends to some extent on the entrance Reynolds number. However, it has been demonstrated (13, 18) that the variation can usually be represented by a simple function of x/D for a wide range of Reynolds numbers. Two different functions have been used to correlate average heat transfer coefficients in the case of a fully developed velocity profile and a flat temperature profile at the start of heating. The first (7,10,13) assumes that the average Nusselt number (up to the length x) varies as $\left(\frac{x}{D}\right)^{-0.1}$ until x/D = 60; beyond this value the Nusselt

*This discussion supersedes Section 3.1 of Technical Report 247-1 (2).

number is essentially constant with x/D. For values of x/D greater than 60, the factor $(x/D)^{-0.1}$ is replaced by the constant $(60)^{-0.1}$. The second method of correlation (18, 22) uses the factor

$$1 + \left(\frac{x}{D}\right)^{-0.7}$$

to express the variation of average Nusselt number with axial position. It should be noted that, at very large x/D, the two functions differ by a factor of $(60)^{-0.1} = 0.664$.

Since the local heat transfer coefficient h, at a point away from the entrance, is always smaller than the average coefficient h_{av} up to that point, the entrance length for the former is considerably shorter than for the latter and the correlations given above can not be rigorously valid for local considerations. However, no entrance length correlations are available for local heat transfer coefficients and Nusselt numbers; either local values are reported only at x/D greater than 60 (the so called "fully developed" values) or one of the average correlations is used without comment.

3.2 CORRELATION OF HEAT TRANSFER DATA*

At moderate temperature differences, it has been customary (13) to correlate heat transfer data for fluids flowing turbulently inside smooth tubes by the equation

$$N_{Nu} = 0.023\ N_{Re}^{0.8} N_{Pr}^{0.4} \qquad 11$$

However, the investigation of Drexel and McAdams (13) suggests that equation 11 should be modified slightly for air, and presumably other gases, to read

$$N_{Nu} = 0.021\ N_{Re}^{0.8} N_{Pr}^{0.4} \qquad 12$$

Equations used to correlate data under conditions of large temperature differences should be compatible with these relations. Compatibility can

*Supersedes Section 3.3 of Technical Report 247-1 (2).

be achieved, as stated previously, either by evaluating all fluid properties at a "film" temperature between the bulk and the surface temperature or by introducing a temperature ratio parameter, T_w/T_b.

Humble, Lowdermilk and Desmon (10), in reporting experimentally measured average heat transfer coefficients for air flowing in smooth heated tubes, give the relation

$$N_{Nu,f,av} = 0.034 \left(N_{Re,f,av}\right)^{0.8} \left(N_{Pr,f,av}\right)^{0.4} \left(\frac{L}{D}\right)^{-0.1} \qquad 13$$

where $(60)^{-0.1}$ was used for values of L/D greater than 60. The subscript f denotes that fluid properties, including the density, were evaluated at a "film" temperature equal to the average of the surface and gas bulk temperatures.* Equation 13 fits the experimental data very well, especially for Reynolds numbers of 10,000 and above. The same relation for average heat transfer coefficients was used by Durham, Neal and Newman (7) for correlating data obtained by heating helium flowing in smcoth tubes. Taylor and Kirchgessner (18) report a slightly different form of the equation for helium flowing in smooth tubes:

$$N_{Nu,f,av} = 0.021 \left(N_{Re,f,av}\right)^{0.8} \left(N_{Pr,f,av}\right)^{0.4} \left[1 + \left(\frac{L}{D}\right)^{-0.7}\right] \qquad 14$$

To correlate local heat transfer coefficients in the fully developed region (x/D greater than 60), Taylor and Kirchgessner used

$$N_{Nu,f} = 0.021 \, N_{Re,f}^{0.8} \, N_{Pr,f}^{0.4} \qquad 15$$

---

*Note that the "modified" Reynolds number is defined by

$$N_{Re,f} = \frac{D\rho u}{\mu_f} \frac{T_b}{T_f}$$

and, for a perfect gas,

$$N_{Re,f} = \frac{D\rho_f u}{\mu_f}$$

which fits their data within ± 38%. Lapides and Goldstein (12), using a corrected value for the thermal conductivity of air, replotted the fully developed local data obtained by the NACA and reported by Deissler and Eian (6). The best fit was given, within approximately ± 10%, by

$$N_{Nu,f} = 0.0205\ N_{Re,f}^{0.8}\ N_{Pr,f}^{0.4} \qquad 16$$

Durham, Neal and Newman report, for helium flowing in smooth tubes, the equation

$$N_{Nu,f} = 0.036\ N_{Re,f}^{0.8}\ N_{Pr,f}^{0.4}\ \left(\frac{x}{D}\right)^{-0.1} \qquad 17$$

which reduces to

$$N_{Nu,f} = 0.024\ N_{Re,f}^{0.8}\ N_{Pr,f}^{0.4} \qquad 18$$

for local Nusselt numbers in the fully developed region.

Correlations of the type above, i.e., those which employ the evaluation of fluid properties at a "film" temperature, tend to obscure the significance of the actual fluid properties. In turbulent flow the velocity and temperature are relatively constant across the turbulent core, and the gas properties, consequently, are also almost constant across this turbulent core. In particular the mass flow velocity G, a quantity which is independent of distance in the axial direction and which is widely used, is not directly employed in the correlations.

These anomalies may be avoided by using a correlation in which the fluid properties are evaluated at gas bulk temperature and into which T_w/T_b is introduced as a parameter (1,14,17). For average Nusselt numbers, Barnes (1) reports the equation

$$N_{Nu,av} = 0.023\ N_{Re,av}^{0.8}\ N_{Pr,av}^{0.4}\ \left(\frac{T_w}{T_b}\right)^{a} \qquad 19$$

where the exponent, a, varies from gas to gas. His investigation gives the following values:

Air	$a = -0.4$
Helium	$a = -0.185$
Carbon Dioxide	$a = -0.27$

At the same time, Barnes states that the data of Humble, et al. (10), suggest $a = -0.55$ for air.

The results of the present tests are compared to both types of correlations discussed, i.e., those using a reference "film" temperature and those employing a temperature ratio parameter.

3.3 LOCAL FRICTION FACTORS

Deissler (3) reports analytically determined friction factors for fully developed, turbulent flow through smooth tubes with heating for a Prandtl number of one. The results indicate that friction factors, for the case of gas heating, fall below the generally accepted Karman-Nikuradse relation for isothermal, turbulent flow,

$$\frac{1}{\sqrt{4f}} = 2 \log(N_{Re}\sqrt{4f}) - 0.8 \qquad 20$$

when the fluid properties are evaluated at gas bulk temperature. Furthermore, it is indicated that this trend is progressively more pronounced at higher values of $\frac{T_w}{T_b}$. The analysis predicts that equation 20 will correlate fully developed flow friction factor data if gas properties are evaluated at a reference temperature, $T_{0.4}$, defined as

$$T_{0.4} = 0.4(T_w - T_b) + T_b \qquad 21$$

Deissler and Eian (6) extended the analysis described above to the case of a Prandtl number of 0.73, and the resulting friction factors were compared to experimentally determined values measured at a position 6 inches from the exit of an 87-inch test section for the flow of air. The results are correlated by equation 20 for Reynolds numbers above 30,000 if the gas properties are evaluated at the reference temperature, $T_{0.4}$. For lower Reynolds numbers, the experimental friction factors fall above those predicted by the equation.

3.4 AVERAGE FRICTION FACTORS

A number of authors (10,18,22) report experimentally determined average friction factors for gases flowing through smooth tubes with high surface to bulk temperature ratios. These results generally indicate that if the fluid properties are evaluated at gas bulk temperature, the average friction factors fall below those predicted by equation 20 for Reynolds numbers above 30,000. These results show that if the fluid properties are evaluated at the average "film" temperature, the friction factors are fairly well predicted by equation 20 for Reynolds numbers above 30,000. At lower Reynolds numbers, the friction factors tend to be progressively higher than those predicted by the Kármán-Nikuradse relation as the ratio $\frac{T_w}{T_b}$ is increased, whether the fluid properties are evaluated at bulk temperature or at a film temperature.

4. EXPERIMENTAL APPARATUS

Heat transfer and pressure drop measurements are made for a gas flowing through a 1/8-inch i.d. by 0.022-inch wall, round, inconel tube with a heated length of 20 inches and an unheated entrance length of 2 1/8 inches. Thermocouples and pressure taps are attached to this test section tube at several axial positions.

The apparatus described in Technical Report No. 247-1(2) was modified for the present experimental program as follows:

1. A support stand for the test section was added.
2. The electrode arrangement was altered.
3. Thermocouple attachment and test section insulation were changed.
4. The entrance gas mixer was placed inside the pressure vessel at the inlet to the test section.
5. Pressure taps were added to the test section, and a pressure drop measuring system was installed.

4.1 TEST SECTION MODIFICATIONS

Figure 1 shows the test section assembly less thermocouples, insulation, and pressure vessel. The support stand consists of three 1/2-inch inconel tubes screwed into the lower flange, two reinforcing brackets, and a plate which supports the upper electrode assembly. A graphite-packed sliding electrode (2) is welded to an inconel plate to which two 3/8-inch diameter, nickel bus bars are welded. This plate is bolted to, but insulated from, the upper plate of the support stand.

A 3/8-inch o.d. by 1/8-inch i.d. tube is brazed onto the upper end of the test section. The tube is free to move vertically in the sliding electrode as thermal expansion of the test section dictates. The support stand protects the test section while the pressure vessel is being lowered into place and serves as a frame for the attachment of the pressure taps and thermocouples.

Chromel-alumel thermocouples are welded to the test section at nine axial locations and are supported by one-inch diameter, alumina segments (Figure 2). These segments are clamped to the test section independently; therefore, they move with the test section as it experiences thermal expansion, and the thermocouples and pressure taps are not torn from the test

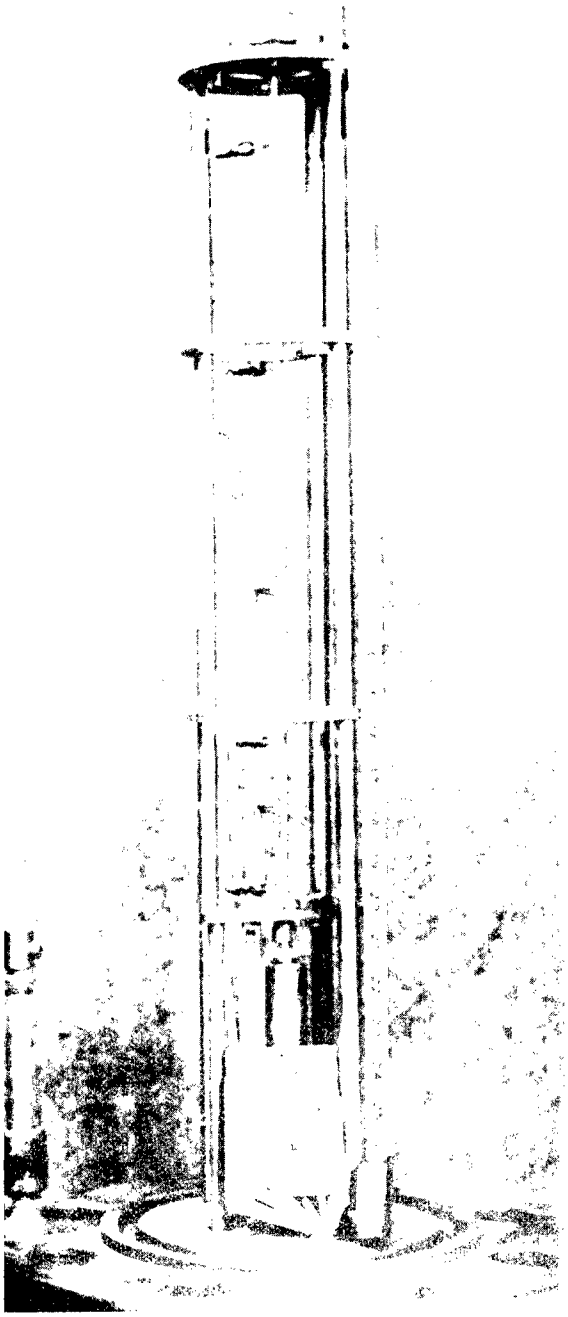

Figure 1 Test Section – Pressure Taps & Support Stand

section. Quartz fiber is placed in the annulus between the segmented insulation and the pressure vessel to reduce the heat loss.

Pressure taps are located along the test section at seven axial positions so that the static pressure variation can be measured as the gas flows through the test section. These pressure taps are 1/16-inch o.d. inconel tubes brazed to the test section with 0.050-inch holes drilled through the test section wall. All burrs inside the test section resulting from the drilling process were removed.

A gas mixer is located inside the pressure vessel so that the gas temperature can be measured immediately upstream from the test section entrance.

4.2 PRESSURE-DROP MEASURING SYSTEM

A bank of twelve 50-inch manometers, a 60-inch inclined manometer, and two 0-1200 psi Bourdon tube pressure gauges are used to measure the static pressure distribution along the test section.

The bank of manometers is so arranged that the static pressure drop between successive pressure taps and between the last pressure tap and the pressure vessel can be measured by 50-inch water manometers; or the successive pressure drops between the last five taps and the pressure vessel can be measured by 50-inch mercury manometers. An additional manifold and valve arrangement permit the measurement of pressure drop between any two taps, or any tap and the pressure vessel, by use of either the 60-inch inclined-tube water manometer; a 50-inch mercury manometer; or two Bourdon tube gauges. With this arrangement, pressure drops from 0.01 inch of water to several hundred psi can be measured.

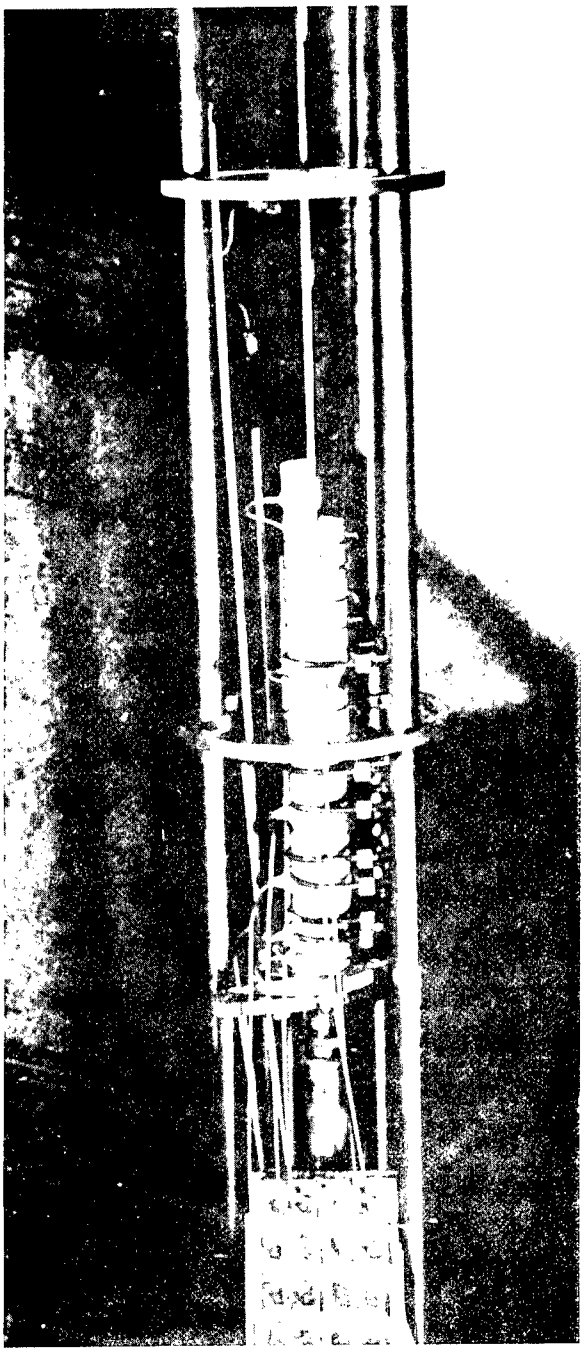

Figure 2 Test Section – Thermocouples & Insulation Segments

5. METHOD OF TESTING

A series of experiments has been performed with nitrogen to determine local heat transfer coefficients and local and average friction factors for gas flowing through tubes of circular cross-section.

The method of testing was the same as reported in Technical Report No. 247-1(2) except as described below. A number of the important experimentally determined quantities are shown in Figures 8 and 9.

5.1 RANGE OF VARIABLES

Heat transfer and pressure drop data were obtained over the ranges of important variables listed in the following table:

RANGE OF VARIABLES

1.	Flow rate	1.24 to 32.6 lb/hr
2.	Inlet gas temperature	approximately 70° F
3.	Maximum gas temperature	784° F
4.	Maximum surface temperature	1455° F
5.	Maximum T_w/T_b	2.08
6.	Bulk Reynolds number	1830 to 90,000
7.	Heat flux	733 to 138,000 Btu/(hr)(sq ft)
8.	Axial location parameter, $\frac{x}{D}$	2 to 127

5.2 THERMOCOUPLE CALIBRATION

The test section temperature at several locations was measured by chromel-alumel thermocouples welded to the outside of the test section. Part of the signal from a given thermocouple was caused by the heating current flow through the test section; i.e., the two wires of the thermocouple were not at exactly the same potential on the test section. This effect was minimized by careful attachment of the thermocouples, but could not be completely eliminated. Each thermocouple was calibrated for this erroneous signal as a function of test section current; a description of the calibration is presented in Appendix A, and a sample resulting calibration curve is shown in Figure 10. A typical test section temperature distribution is shown in Figure 8. Inside wall temperatures were calculated as described in Appendix B.

5.3 HEAT LOSS CALIBRATION

The data for heat loss calibration were taken the same way as reported in reference 2; however, the interpretation of the heat loss and subsequent application of the results to the experiments were refined as discussed in Appendix C.

5.4 HEAT FLUX TO THE GAS

The total power input to the test section was measured as described in reference 2 except that the voltage drops between the lower electrode and the pressure taps were measured; these showed that the voltage varied linearly along the test section. The conversion of electrical energy to thermal energy, consequently, was uniform along the test section. The calculation of the heat loss is described in Appendix C, and the difference between the heat generation per unit length and the heat loss per unit length is the heat transferred to the gas per unit length. A typical plot of heat flux to the gas as a function of $\frac{x}{D}$ is shown in Figure 8.

5.5 GAS TEMPERATURE

The inlet gas temperature was measured in a mixer inside the pressure vessel just at the test section entrance. Gas bulk stagnation temperature at any axial location was calculated by equating the increase in enthalpy of the gas to the integrated heat transfer to the gas, up to that point, and then using an enthalpy curve (Figure 11) to determine the temperature.

The static enthalpy, H, at each axial location was then calculated from the energy equation,

$$H = H_o - \frac{u^2}{2g_c J}$$

where H_o is the stagnation enthalpy (at the known stagnation temperature) and u is the average velocity at the location as determined from the continuity equation, $w = \rho A u$, and the equation of state for nitrogen, $\rho = \rho(P, T)$. The static temperature was read from a plot of H vs T with pressure as a parameter. Since the density is a function of static temperature, the density and average velocity could not be found until the static temperature was known. Therefore, it was necessary to use an iterative procedure: the

static temperature was estimated, density and velocity determined, and, from the static enthalpy, a corrected temperature was found. The calculation converged very rapidly, only two or three cycles being required at each location.

In addition the adiabatic wall temperature was calculated by the equation,

$$T_{aw} = T + R(T_o - T) = T + N_{Pr}^{a}(T_o - T)$$

given in reference 15 where the exponent, a, is 1/3 for turbulent flow and 1/2 for laminar flow. The turbulent value was used for all runs; however, no significant error was hereby introduced in the low Reynolds number runs as the maximum difference between static and stagnation temperatures was only 37° F.

5.6 PRESSURE DROP

The pressure drops between successive pressure taps and between the last tap and the pressure vessel were measured during each run. The combination of manometer bank, inclined manometer, and Bourdon tube gauges was used in such a manner as to measure each pressure drop with maximum available sensitivity; i.e., the inclined manometer was used to measure pressure drops from 0 to 10 inches of water, the water manometers to measure pressure drops from 10 to 50 inches of water, the mercury manometers to measure pressure drops from 50 inches of water to 50 inches of mercury, and the Bourdon tube gauges to measure pressure drops greater than 50 inches of mercury. Figure 8 shows a typical curve of static pressure variation along the test section with the vessel pressure as the datum.

5.7 HEAT TRANSFER COEFFICIENTS

Using the calculated heat flux to the gas, q''_w, and the temperature difference, $T_w - T_{aw}$, the local heat transfer coefficient, h, was calculated from equation 1,

$$h = \frac{q''_w}{T_w - T_{aw}}$$

A typical plot of the heat transfer coefficient for a test is shown in Figure 9.

5.8 FRICTION FACTORS

Average friction factors were calculated from equations 8 and 9 with the two stations being pressure taps 1 and 7. Local friction factors were calculated from equations 5 and 6. The term, $\frac{d}{dx}\left[P + \frac{\rho u^2}{g_c}\right]$, was evaluated at selected thermocouple positions by plotting $P + \frac{\rho u^2}{g_c}$ as a function of x and then graphically differentiating the resulting curve at the position of interest. A typical plot of local friction factor as a function of $\frac{x}{D}$ is shown in Figure 9.

5.9 GAS PROPERTIES

Four properties of nitrogen were used in the calculations: enthalpy, viscosity, thermal conductivity, and Prandtl number. These properties were evaluated at the associated static bulk or film temperature except in determining the stagnation enthalpy where, by definition, the stagnation temperature must be used. Figures 11 through 14 in Appendix E show these properties' variation with temperature, and the important references are listed.

6. EXPERIMENTAL RESULTS

The results of the present experimental investigation are graphically summarized in Figures 3, 4, and 5 and are discussed in detail below. The heat transfer results are presented in two ways. In the first (Figure 3), the gas properties are evaluated at the "film" temperature, as defined in Section 3. In the second method (Figure 4), the bulk static temperature of the gas is used for property evaluation and the temperature ratio, T_w/T_b, is introduced as a parameter. Fully developed local friction factors are presented in Figures 5 and 6 with gas properties evaluated at bulk and film temperature respectively. Figure 7 is a plot of average friction factors. In addition, Figures 8 and 9 show representative axial distributions of the more important experimental variables.

Because of their large uncertainties, the data obtained with an earlier test section and presented in Technical Report 247-1(2) are not included in the present report. In general, the heat transfer correlations used in report 247-1 lie somewhat above those discussed below in Sections 6.1 and 6.2.

6.1 HEAT TRANSFER CORRELATION BASED ON FILM TEMPERATURE

The local heat transfer data are correlated, as shown in Figure 3, by plotting the quantity

$$\frac{N_{Nu,f}}{N_{Pr,f}^{0.4}\left[1+\left(\frac{x}{D}\right)^{-0.7}\right]}$$

as a function of the film Reynolds number. The best fit to the data was given by

$$N_{Nu,f} = 0.019\, N_{Re,f}^{0.8}\, N_{Pr,f}^{0.4}\left[1+\left(\frac{x}{D}\right)^{-0.7}\right] \qquad 22$$

which is shown as a solid line. The two dashed lines indicate 10 per cent deviation from this equation. The bulk of the data falls within the $\pm$ 10 per cent interval, the exceptions being data points from the two thermocouples at $\frac{x}{D}$ smaller than 6, where axial conduction heat losses are large.

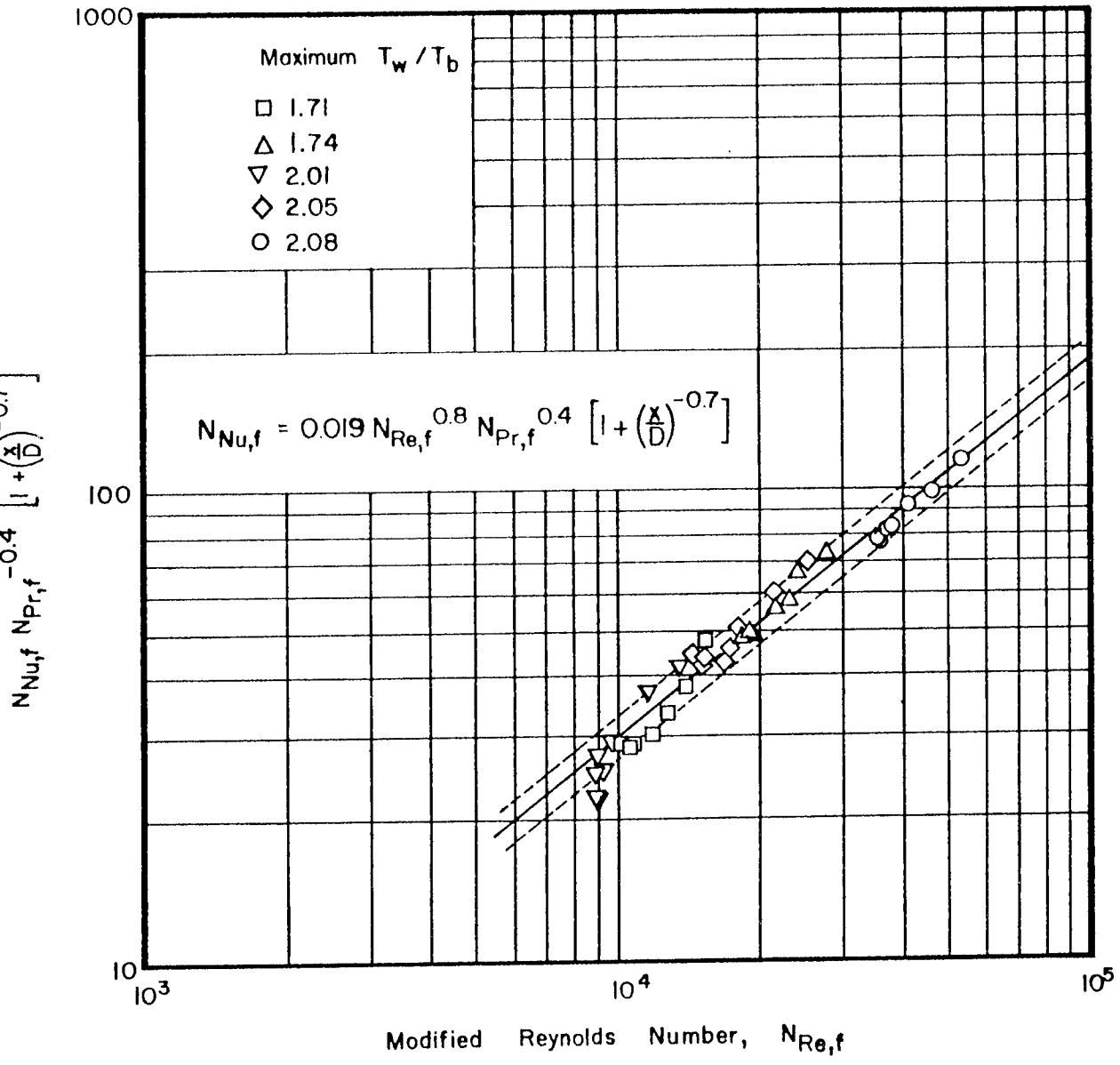

Figure 3 Heat Transfer Correlation Based on Local Values, Fluid Properties Evaluated at Reference Temperature, T_f

Only those runs with film Reynolds numbers greater than 8000 are plotted. However, the tendency of the data to fall below the turbulent flow correlation at low Reynolds numbers is already evident. This trend is to be expected as the flow may be transitory between the laminar and turbulent regimes of flow.

The experimental curve (equation 22) is slightly lower than those reported by other investigators, but it agrees, within the spread of the data, with equation 16 for air (12) and equation 15 for helium (18). Equations 17 and 18 taken from Durham, Neal and Newman (7) lie considerably above the present experimental correlation and others cited.

6.2 HEAT TRANSFER CORRELATION BASED ON T_w/T_b PARAMETER

The local heat transfer data are correlated in terms of the parameters N_{Nu}, N_{Re}, N_{Pr}, $\frac{x}{D}$ and T_w/T_b by plotting the quantity

$$\frac{N_{Nu}\left(\frac{T_w}{T_b}\right)^{0.5}}{N_{Pr}^{0.4}\left[1+\left(\frac{x}{D}\right)^{-0.7}\right]}$$

as a function of the Reynolds number in Figure 4. All data obtained in the present investigation are included in this figure, including those near the entrance where x/D is 2. The solid line represents

$$N_{Nu} = 0.020\ N_{Re}^{0.8}\ N_{Pr}^{0.4}\left(\frac{T_w}{T_b}\right)^{-0.5}\left[1+\left(\frac{x}{D}\right)^{-0.7}\right] \qquad 23$$

the best fit to the data with Reynolds numbers greater than 10,000, and the dashed lines indicate 10 per cent deviation from this equation. Again, the data with Reynolds number greater than 10,000 are correlated within $\pm$ 10 per cent, while the two data points on each run where $\frac{x}{D}$ is less than 6 tend toward greater scatter.

The range of values of T_w/T_b in the present experimental results (maximum of 2.1) was insufficient to check the generality of the exponent -0.5 appearing on T_w/T_b in equation 23. However, the data do indicate that the value is somewhat greater than the -0.4 reported by Barnes (1) for air.

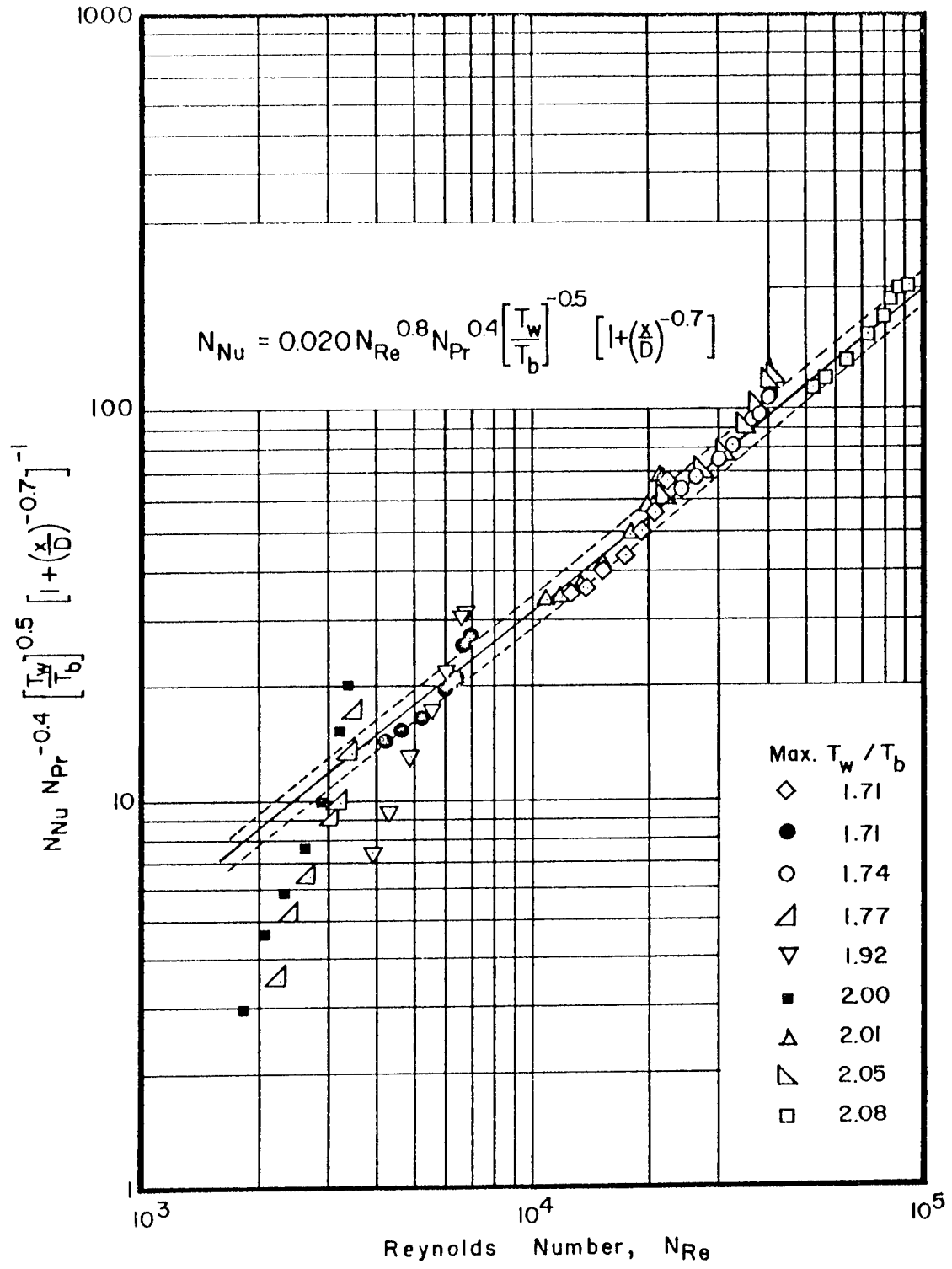

Figure 4 Heat Transfer Correlation Based on Local Values, Fluid Properties Evaluated at Bulk Temperature

6.3 THERMAL ENTRANCE REGION

Both of the entrance parameters discussed in Section 3.1,

$$\left(\frac{x}{D}\right)^{-0.1} \quad \text{and} \quad \left[1 + \left(\frac{x}{D}\right)^{-0.7}\right]$$

were investigated as means of correlating the experimental data. There is no noticeable difference between the two parameters for $\frac{x}{D}$ greater than 6. At smaller $\frac{x}{D}$, the two diverge with $\left(\frac{x}{D}\right)^{-0.1}$ falling well below $\left[1 + \left(\frac{x}{D}\right)^{-0.7}\right]$. On the other hand, the data points from the first two thermocouples ($\frac{x}{D}$ = 1.76 and 5.76) lie slightly above the values predicted using the latter parameter. Consequently, $\left[1 + \left(\frac{x}{D}\right)^{-0.7}\right]$ was chosen for the two heat transfer correlation equations.

6.4 FRICTION FACTORS

The experimentally determined friction factors are plotted vs Reynolds number on Figures 5, 6, and 7 with Kármán-Nikuradse relation for isothermal, turbulent flow through smooth tubes and the laminar flow relation, $f = \frac{16}{N_{Re}}$, included for reference. The results of a series of tests performed to measure average friction factors with no gas heating are shown in Figure 7 and indicate that the test section may be considered as a smooth tube for friction factor measurements.

Local friction factors as defined by equation 5 were determined at each thermocouple location, and Figure 9 shows a plot of friction factor variation along the test section for a typical run. As can be seen in the figure, the friction factor increases in the direction of flow in the thermal entrance region and then decreases in the direction of flow toward the exit. The large variation in the friction factor along the test section clearly illustrates that the pressure drop is significantly affected by the heat transfer process, in addition to the effect of a simple change in the momentum of the gas. It is also evident that the flow cannot be considered "fully developed" in a rigorous sense, even at large values of $\frac{x}{D}$, as far as the friction factors are concerned.

The friction factors calculated at thermocouple number 7 ($\frac{x}{D}$ = 96), which is as near the exit as end effects can be neglected for all runs, are plotted vs Reynolds number with gas properties calculated at bulk temperature

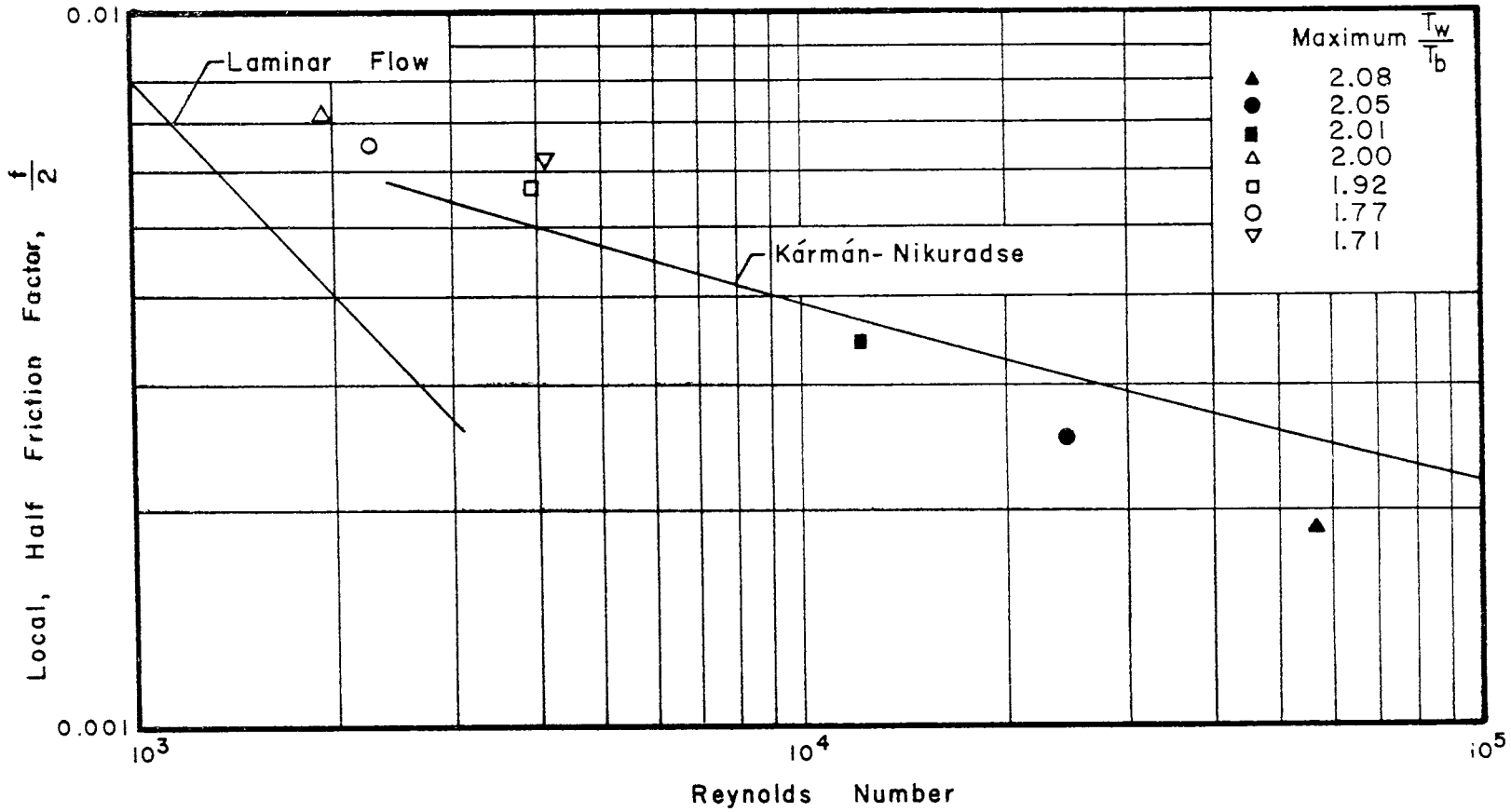

Figure 5 Friction Factor Correlation Based on Local Values, Fluid Properties Evaluated at Bulk Temperature

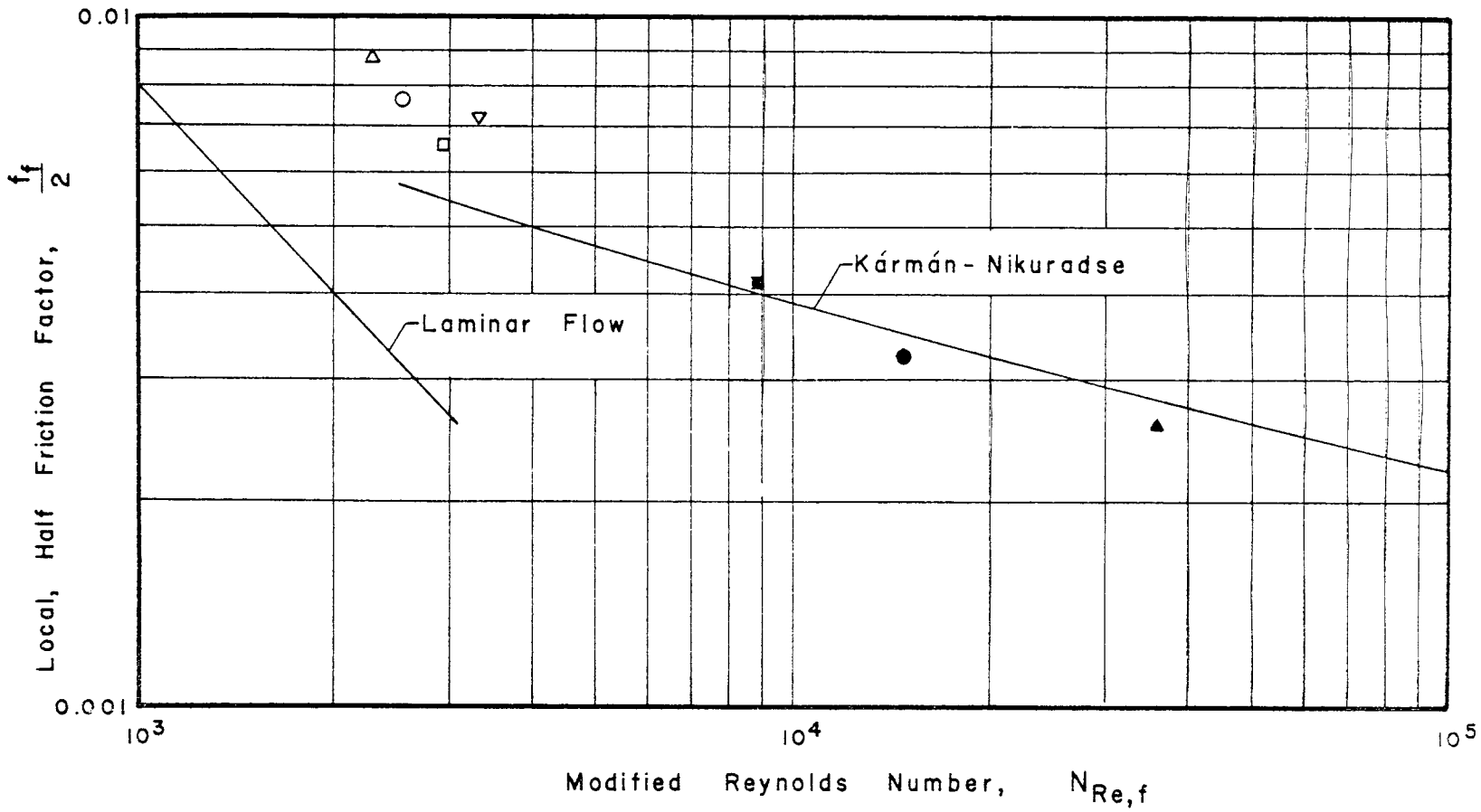

Figure 6 Friction Factor Correlation Based on Local Values, Fluid Properties Evaluated at Reference Temperature, t_f

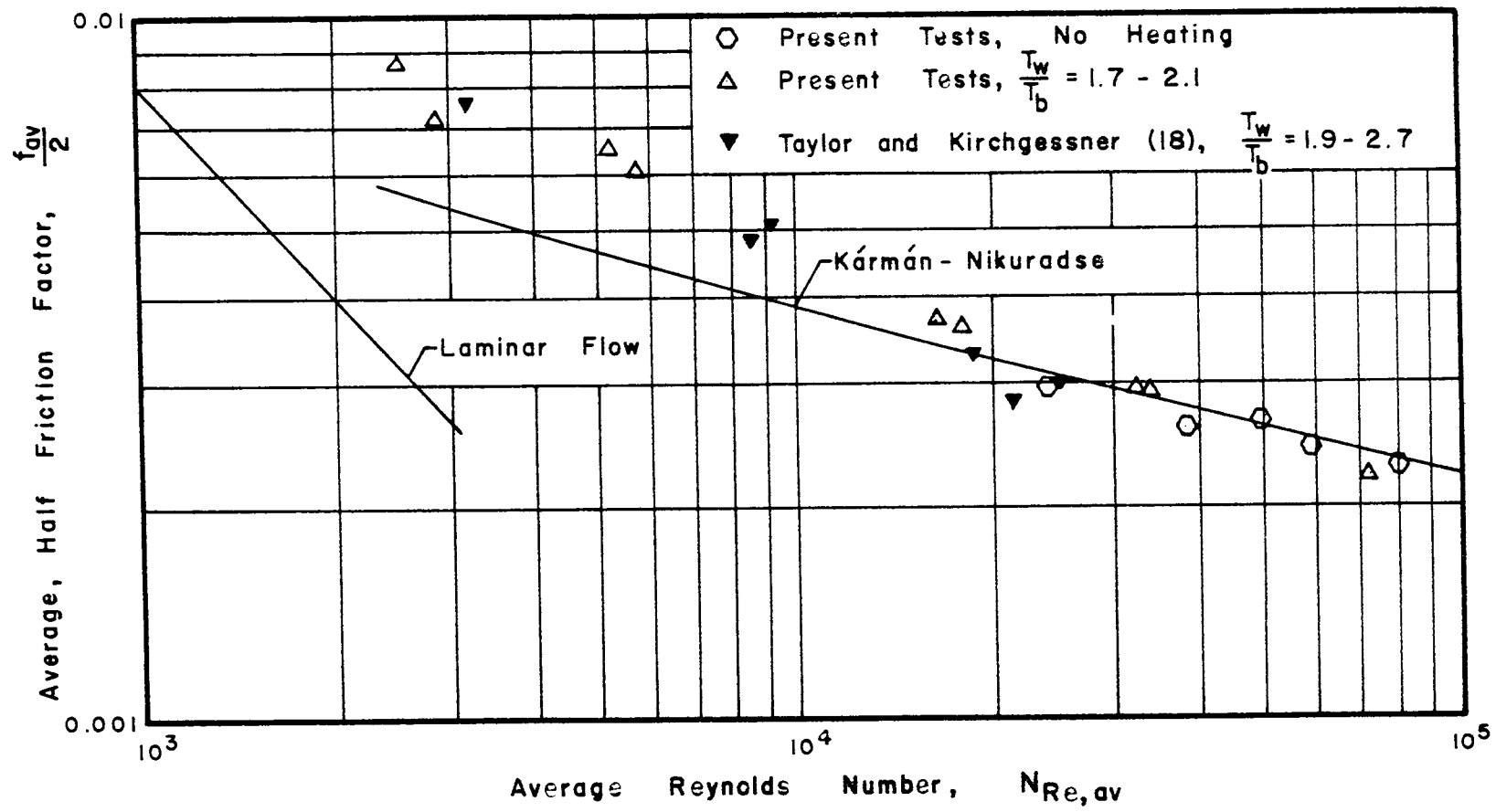

Figure 7 Friction Factor Correlation Based on Average Values, Fluid Properties Evaluated at Bulk Temperature

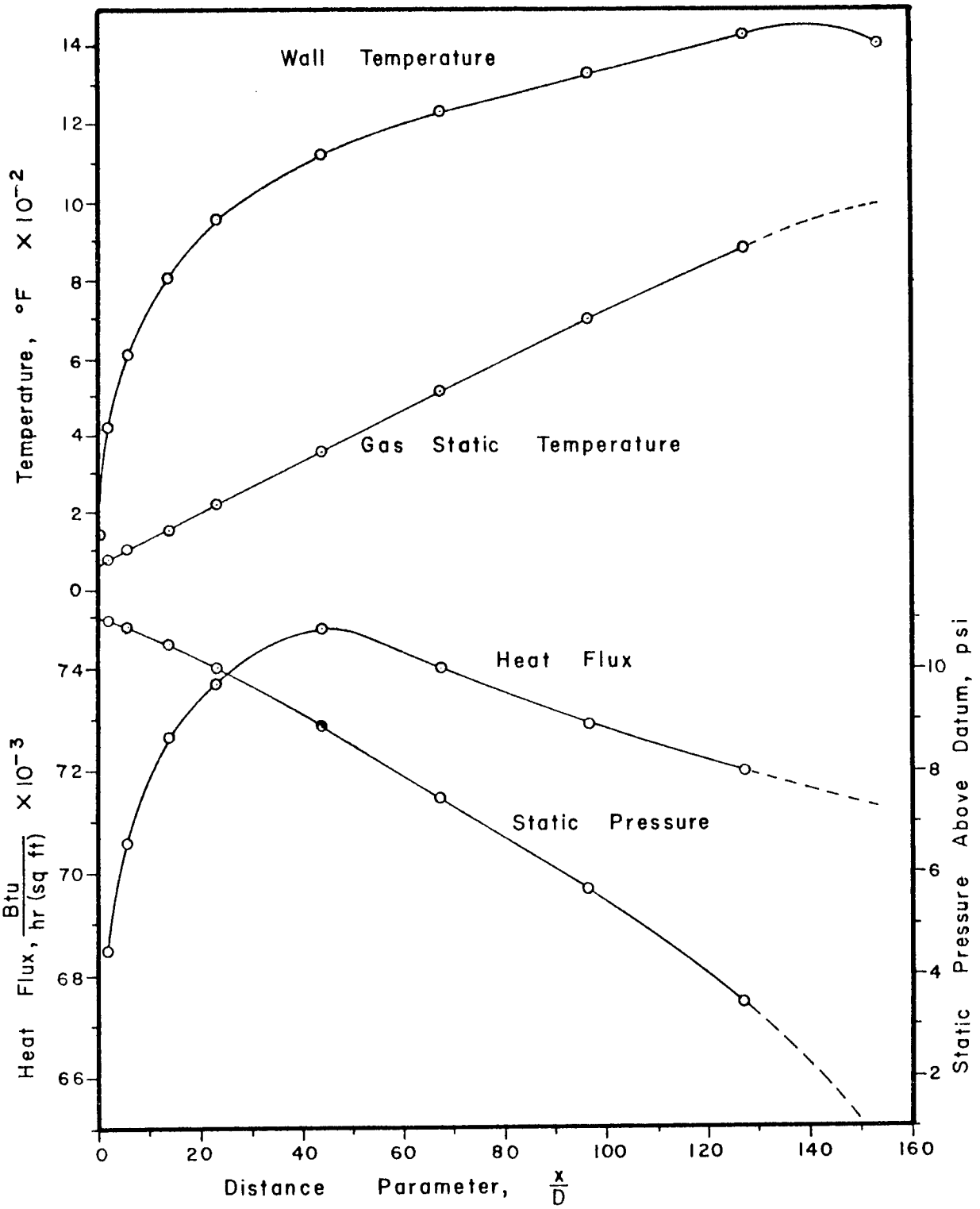

Figure 8 Heat Flux, Temperature, and Pressure Distributions for a Typical Test

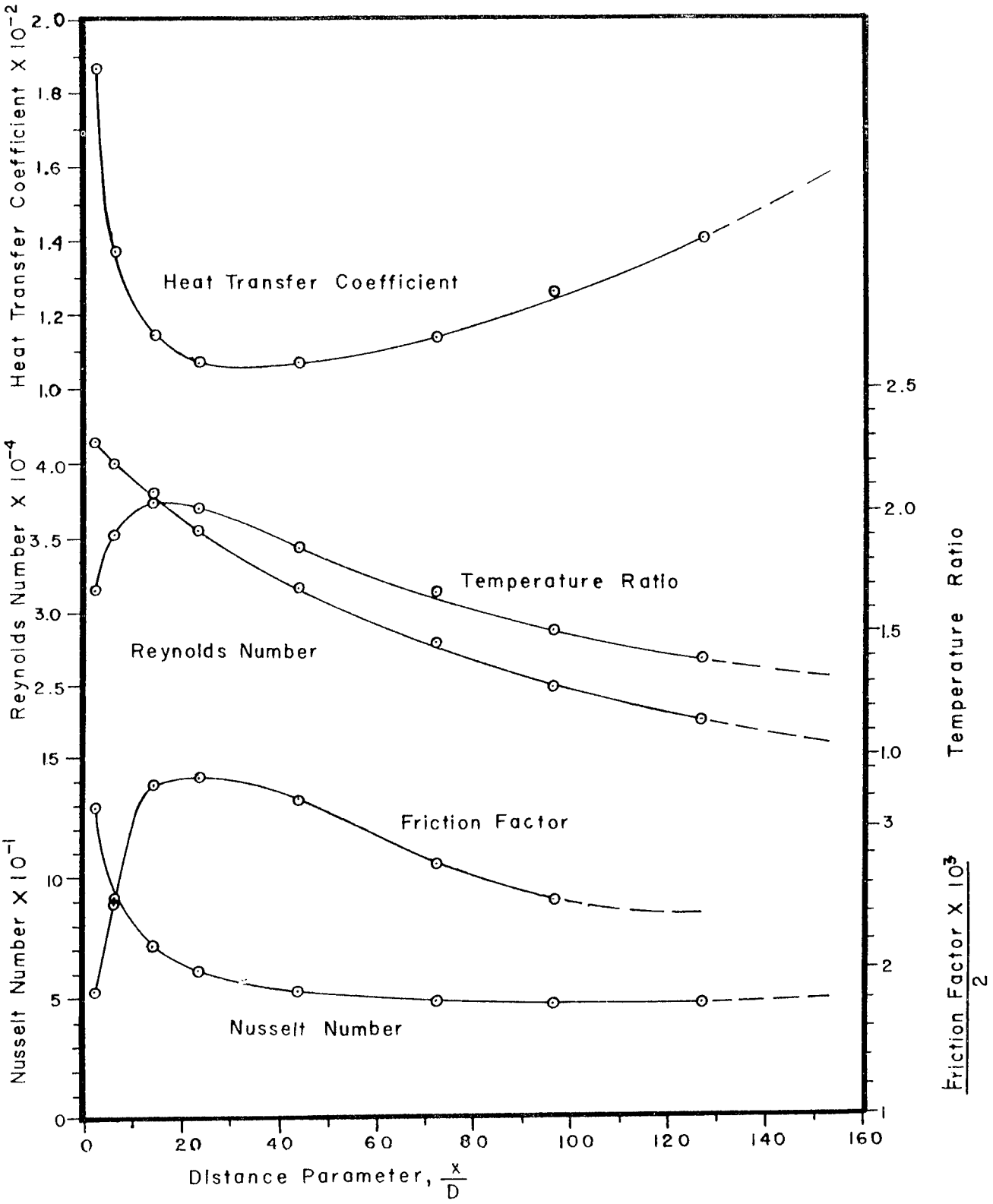

Figure 9 Heat Transfer Coefficient, Friction Factor, Nusselt Number, Reynolds Number, and Temperature Ratio Variation for a Typical Test

in Figure 5. For Reynolds numbers above 10,000, the results are substantially in agreement with those predicted by Deissler (5) for fully developed flow in that the friction factors are lower than would be calculated by equation 20. At the lower Reynolds numbers, the friction factors are considerably higher than those predicted by equation 20 or the laminar flow relation. Figure 6 shows the same points but with the fluid properties evaluated at a reference temperature, T_f; the results are correlated by equation 20 for Reynolds numbers above 10,000 and are above the correlation for lower Reynolds numbers. These same trends are observed in the results of Deissler and Eian (6).

Figure 7 shows the average friction factor as a function of the Reynolds number with all fluid properties evaluated at the average gas bulk temperature. The results of Taylor and Kirchgessner (18) are also plotted on the figure. For Reynolds numbers above 20,000, the friction factors are slightly below the Kármán-Nikuradse relation; and for lower Reynolds numbers, the friction factors are considerably above this relation as well as above the laminar relation. No attempt was made to correlate average friction factor data with fluid properties evaluated at an average reference temperature because there is no significant average reference temperature when the conditions are changing so much along the test section (Figures 8 and 9).

6.5 EXPERIMENTAL UNCERTAINTY

The uncertainties in the reported experimental results were determined from the estimated uncertainty intervals associated with the various primary measurements. Estimates of the various uncertainty intervals were obtained from instrument specifications and calibrations, observed measurement fluctuations, and operator judgement. A detailed uncertainty analysis, after the method of reference 11, is presented in Appendix D. The numerical values of the uncertainty intervals obtained are reasonable estimates of typical intervals for the present tests.

An uncertainty interval of $\pm$ 9.5 per cent was found for the heat transfer coefficients and is reliable except for the results obtained near the lower electrode, where the uncertainty interval is considerably larger because of the significant axial conduction heat losses.

The uncertainty interval in the friction factors is $\pm$ 12 per cent, and the controlling item is the numerical or graphical differentiation necessary to evaluate the apparent wall shear stress from equation 7.

APPENDIX A. THERMOCOUPLE CALIBRATION

Thermocouples in electrical contact with current-carrying conductors will produce a voltage signal consisting of two parts: the desired emf which is approximately proportional to the temperature difference between the hot and cold junctions, and an extraneous component which occurs because the two wires constituting the thermocouple junction are not at the same electrical potential on the conductor. In order to determine the temperature in such a situation, the extraneous signal must be measured or eliminated. For example, if the current in the conductor is alternating, an R-C filter circuit may be devised to attenuate this component.

In welding the thermocouples to the test section, care was taken to keep the two wires at the same electrical potential by trimming the junction and carefully positioning it on the test section before welding. Since this procedure did not completely eliminate the extraneous signal, a method of calibration was devised to measure it accurately as a function of test section current and temperature.

The extraneous signal was measured by passing a steady heating current of up to 300 amperes through the test section while continuously recording the total thermocouple emf and the heating current on an oscillograph. The current flow was then interrupted suddenly by opening a 300-ampere circuit breaker, after which the thermocouple emf no longer included the extraneous component. Figure 10a shows a replica of a typical oscillograph trace from such a test, from which it may be seen that the cooling of the test section after the interruption of heating current is slow compared to the rate of change of heating current. Consequently, the sudden change in thermocouple emf, which may be positive or negative, is entirely attributable to the extraneous pickup.

The calibration procedure described above was repeated several times for each thermocouple with different values of heating current and wall temperature. Figure 10b shows the extraneous signal plotted as a function of the current for one thermocouple with wall temperatures from 85 to 1270°F. From tests such as these on all the thermocouples, it is concluded that the pickup from the test section varies linearly with heating current and is independent of temperature.

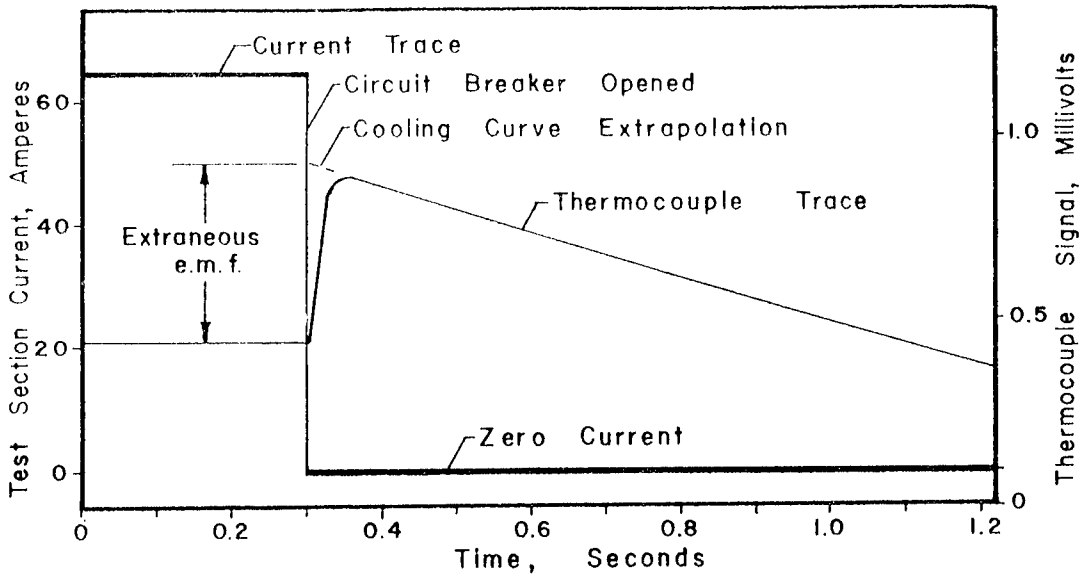

Figure 10a Thermocouple Calibration, Typical Oscillograph Record

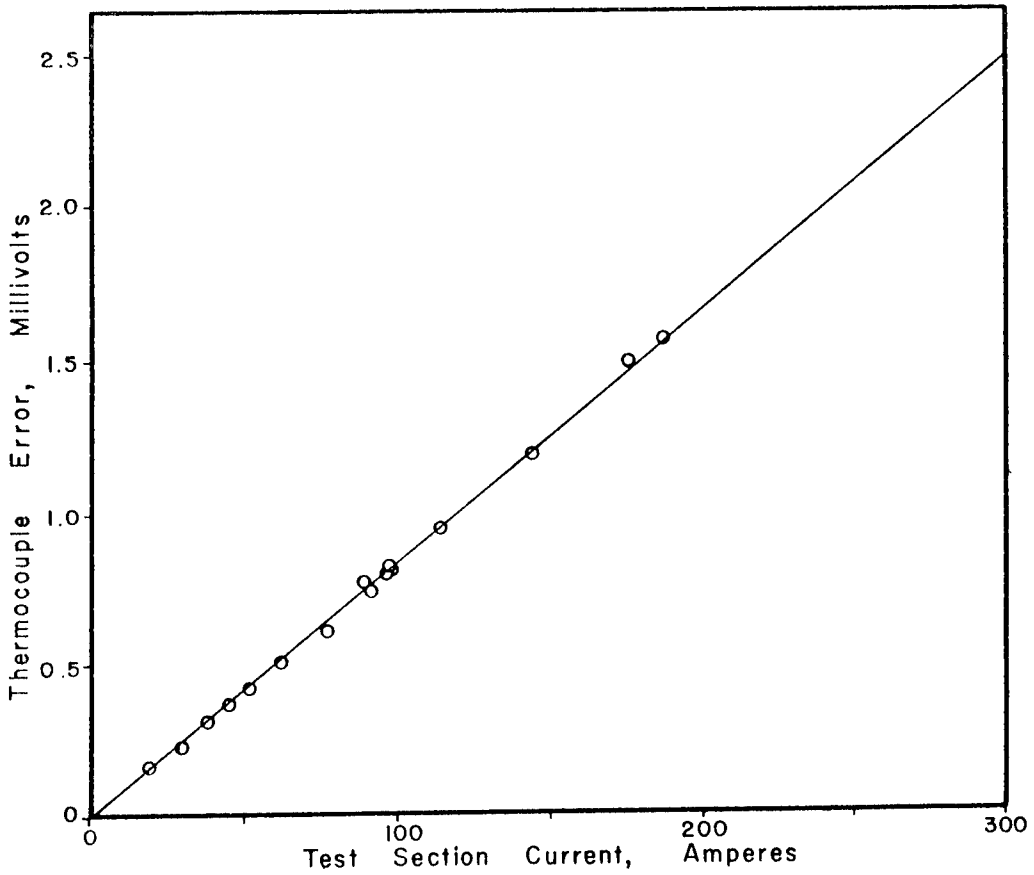

Figure 10b Thermocouple Calibration, Typical Calibration Chart

APPENDIX B. INSIDE SURFACE TEMPERATURE

Thermocouples welded to the outside of the test section tube are the only means of test section temperature measurement. To obtain inside surface temperatures, it is, of course, necessary to correct these temperature measurements for temperature variation across the wall of the test section. The method of correction described below was also used in Technical Report 247-1(2) with the exception that, in Report 247-1, the axial conduction heat loss was neglected.

Since the test section assembly is symmetric with respect to the angular coordinate at a given axial location, the conduction equation for the test section is independent of the angular coordinate. If axial conduction is neglected (this term is small except near the upper and lower electrodes), the conduction equation will be independent of the axial coordinate and the equation may be written as

$$\frac{d^2T}{dr^2} + \frac{1}{r}\frac{dT}{dr} = -\frac{q'''}{k_t} \qquad \text{B-1}$$

where T is the local temperature in the tube wall, r is the radial coordinate, k_t is the thermal conductivity of the tube material, and q''' is the heat generated per unit volume of tube material, by the electrical energy dissipated in the test section.

If uniform heat generation is assumed and the following boundary conditions are used,

(a) $q''_{wo} = q''_r$ (from heat loss calibration)

(b) $T_{wo} = T$ (from thermocouples)

the solution to equation B-1 is

$$T_w = T_{wo} + \frac{q'''}{4k_t}(r_{wo}^2 - r_w^2) - \frac{q'''}{2k_t} r_{wo}^2 \ln\frac{r_{wo}}{r_w} + \frac{r_{wo}}{k_t} q''_r \ln\frac{r_{wo}}{r_w} \qquad \text{B-2}$$

where r_w and r_{wo} are the inside and outside radii of the test section, respectively.

The effect of axial conduction near the electrodes was approximated by lumping the axial heat loss with the radial loss. That is, the first boundary condition was modified as follows:

$$(a') \quad q''_{wo} = q''_r + q''_a$$

Correspondingly, equation B-2 was changed to

$$T_w = T_{wo} + \frac{q'''}{4k_t}(r_{wo}^2 - r_w^2) - \frac{q'''}{2k_t} r_{wo}^2 \ell n \frac{r_{wo}}{r_w} + \frac{r_{wo}}{k_t}(q''_r + q''_a)\ell n \frac{r_{wo}}{r_w} \quad \text{B-2a}$$

This equation was used to calculate the inside surface temperature, T_w, from the experimental data.

APPENDIX C. HEAT LOSS CALIBRATION

At steady state, the energy added to the gas per unit length of test section, q'_w, must equal the total energy generated in the test section per unit length, q'_T, minus the two heat losses: radial loss through the surrounding insulation, q'_r, and axial loss by conduction along the inconel test section, q'_a. Thus, at any axial position along the test section,

$$q'_w = q'_T - (q'_r + q'_a) \qquad C\text{-}1$$

The independent determination of the two heat losses is the subject of this appendix.

It was found convenient to consider the test section tube in two parts, a section close to the lower electrode ($x/D \leq 10$), where axial conduction is of great importance, and a central section ($x/D > 10$) where axial loss is much less than radial loss. The part of the tube near the upper electrode was not considered as no data were obtained closer than four inches to this end of the test section.

C.1 CENTRAL REGION, x/D GREATER THAN 10

Calibration runs were made in which power was supplied to the test section with stagnant gas inside (i.e., no flow). For these runs, all energy generated in the test section must be dissipated either radially through the insulation or axially through the electrodes.

$$q'_T = q'_r + q'_a \qquad C\text{-}2$$

The corrected wall temperature profiles were carefully plotted and the second axial derivative, $\frac{\partial^2 T_{wo}}{\partial x^2}$, at each thermocouple location, was graphically calculated. Since there was only a small variation in temperature across the tube wall at any location, the axial heat loss was estimated as

$$q'_a = -k_t A_t \frac{\partial^2 T_{wo}}{\partial x^2} \qquad C\text{-}3$$

where k_t is the thermal conductivity of the inconel tube and A_t is the cross sectional area of the tube. In all cases, q'_a was quite small compared to q'_T, of the order of 10 per cent or less.

The radial heat loss was then calculated from equation C-2, and a secondary quantity, $U(T_{wo},x)$, defined by

$$q'_r = U(T_{wo},x)\ [T_{wo} - T_{amb}] \qquad C-4$$

was plotted as a function of wall temperature at each thermocouple location.

Thus, for a test run, the radial heat loss at each thermocouple position could be calculated from the measured wall temperature and the calibration curve of $U(T_{wo},x)$. The axial heat loss could be determined in the same manner as for the calibration runs.

C.2 ENTRANCE REGION, x/D LESS THAN 10

Axial heat loss is of primary importance in the entrance region. At thermocouple no. 2 (x/D = 5.76), the axial loss is approximately equal to the radial loss, and at thermocouple no. 1 (x/D = 1.76) the axial loss is more than twice the radial loss.

Since, in this region, the accuracy with which the second derivative could be determined was poor, an equation of the form:

$$T_{wo}(x) = B[1 - e^{-Ax}] \qquad C-5$$

was fitted to each temperature profile in the entrance region. The second axial derivative was then calculated as

$$\frac{\partial^2 T_{wo}}{\partial x^2} = -BA^2\ e^{-Ax} \qquad C-6$$

and the axial heat loss as

$$q'_a = k_t A_t\ BA^2\ e^{-Ax} \qquad C-7$$

A semi-analytical method was used to determine the radial heat loss. The insulation surrounding the test section was considered as a cylinder of

length L with an inside radius equal to that of the test section, r_{wo}, and an outside radius extending to infinity. Assuming constant thermal conductivity, the differential equation for the steady state temperature distribution in the insulation was

$$\frac{\partial^2 T}{\partial r^2} + \frac{1}{r}\frac{\partial T}{\partial r} + \frac{\partial^2 T}{\partial x^2} = 0 \qquad \text{C-8}$$

The following boundary conditions, approximating the physical situation near the lower electrode and test section, were set:

1. At the lower electrode (x = 0), the temperature is constant and equal to the experimentally measured lower electrode temperature.

2. At large distances from the test section ($r \to \infty$), the insulation temperature approaches that of the lower electrode. Actually, it approaches an ambient value; however, this assumption greatly simplifies the solution and introduces little error at the test section near the lower electrode where the solution is applied.

3. At the inside surface of the cylinder ($r = r_{wo}$), the temperature is that of the test section as given by the expression

$$T_{wo} = B[1 - e^{-Ax}]$$

4. At $x = L$, $\frac{\partial T}{\partial x} = 0$.

With these boundary conditions, the solution of equation C-8 is a Fourier sine series of the form

$$T(r,x) = \sum_{n=o}^{\infty} A_n \sin\left(\frac{n\pi}{2L} x\right) K_o\left(\frac{n\pi}{2L} r\right) \qquad \text{C-9}$$

where $K_o\left(\frac{n\pi}{2L} r\right)$ is the zero order, modified Bessel function of the second kind. Since the radial heat loss at the test section must equal the radial heat flow into the insulation,

$$q'_r = -k_{eff}\,(2\pi r_{wo})\left.\frac{\partial T}{\partial r}\right|_{r=r_{wo}} = -2\pi r_{wo} k_{eff} \sum_{n=o}^{\infty} A_n \sin\left(\frac{n\pi}{2L} x\right)\left(\frac{n\pi}{2L}\right)\left[K_1\left(\frac{n\pi}{2L} r_{wo}\right)\right] \qquad \text{C-10}$$

where $K_1\left(\frac{n\pi}{2L} r_{wo}\right)$ is the first order, modified Bessel function of the second kind.

The effective thermal conductivity of the insulation, k_{eff}, was determined from the calibration (no flow) runs by solving equation C-10 using the first seven terms of the series. (Actually, the first four terms were used as all terms with n even are zero.) Then, with k_{eff} known, equation C-10 was used to calculate radial heat losses at the first two thermocouples for the experimental runs.

APPENDIX D. UNCERTAINTY ANALYSIS

The method and terminology in the following analysis follow those of Kline and McClintock (11); the rationale of the procedure is described in Appendix I of Technical Report 247-1 (2).

HEAT TRANSFER COEFFICIENTS

It is necessary to examine separately the variables in the equation defining the heat transfer coefficient,

$$h = \frac{q''_w}{T_w - T_{aw}} \qquad \text{D-1}$$

Let δ G represent the uncertainty interval of a variable G; then by the the method of reference 11,

$$\frac{\delta h}{h} = \sqrt{\left(\frac{\frac{\partial h}{\partial q''_w}\delta q''_w}{h}\right)^2 + \left(\frac{\frac{\partial h}{\partial T_w}\delta T_w}{h}\right)^2 + \left(\frac{\frac{\partial h}{\partial T_{aw}}\delta T_{aw}}{h}\right)^2} \qquad \text{D-2}$$

and substituting from equation D-1,

$$\frac{\delta h}{h} = \sqrt{\left(\frac{\delta q''_w}{q''_w}\right)^2 + \left(\frac{\delta T_w}{T_w - T_{aw}}\right)^2 + \left(\frac{\delta T_{aw}}{T_w - T_{aw}}\right)^2} \qquad \text{D-3}$$

The heat flux to the gas, q''_w, can be expressed as

$$q''_w = \frac{q'_T - q'_r - q'_a}{A_w}$$

where q'_T is the total power supplied per unit length of test section, q'_r is the radial heat loss per unit time per unit length, q'_a is the axial heat loss per unit time per unit length, and A_w is the inside surface area per unit length. The uncertainty in the area A_w can be neglected in comparison with the uncertainties in the energy terms. Thus, the percentage uncertainty in the heat flux to the gas can be expressed as

$$\frac{\delta q''_w}{q''_w} = \sqrt{\left(\frac{\delta q'_T}{q'_T - q'_r - q'_a}\right)^2 + \left(\frac{\delta q'_r}{q'_T - q'_r - q'_a}\right)^2 + \left(\frac{\delta q'_a}{q'_T - q'_r - q'_a}\right)^2} \qquad \text{D-4}$$

Since the values of q'_a were small compared to q'_T, except near the ends of the heated section, the last term can be neglected over most of the test section. However, near the lower electrode (small x/D), the magnitude of q'_a, coupled with its large uncertainty, resulted in a very high heat flux uncertainty, $\frac{\delta q''_w}{q''_w}$.

The uncertainty in the stagnation temperature of the gas can be calculated as described in Technical Report No. 247-1 (2). The final expression for the absolute uncertainty in the stagnation temperature is

$$\delta T_{b,o} = \sqrt{(\delta T_{b,e})^2 + \left(\frac{\delta \bar{q}'_w}{wcp}\right)^2 + \left(\frac{\bar{q}'_w}{wcp}\ \frac{\delta w}{w}\right)^2} \qquad \text{D-5}$$

where $T_{b,e}$ is the temperature of the gas entering the test section and $\bar{q}'_w$ is the average heat transfer to the gas per unit length. The absolute uncertainties of the static and adiabatic wall temperature can be assumed equal to that of the stagnation temperature. The absolute uncertainties, introduced apart from that in the stagnation temperature, are negligible, since the three temperatures, $T_{b,o}$, T_b and T_{aw} differ by less than $40^\circ F$.

As in reference 2, the inside surface temperature of the test section may be calculated by the equation

$$T_w = T_{wo} + \text{correction term}$$

The correction term is small, so a large uncertainty in it would not substantially affect the uncertainty in T_w; therefore, the uncertainty in T_w will be taken as the same as that in T_{wo}.

FRICTION FACTORS

The defining equation for the friction factor can be written as

$$f = \frac{\tau_w}{\frac{\rho u^2}{2g_c}} = \frac{\tau_w}{\frac{G^2}{2\rho g_c}}$$

Thus, the percentage uncertainty in the friction factor may be written as

$$\frac{\delta f}{f} = \sqrt{\left(\frac{\delta \tau_w}{\tau_w}\right)^2 + 4\left(\frac{\delta G}{G}\right)^2 + \left(\frac{\delta \rho}{\rho}\right)^2} \qquad \text{D-6}$$

The uncertainty in the mass flow velocity G is due to the uncertainty in the flow rate w, hence $\frac{\delta G}{G} = \frac{\delta w}{w}$. Using the perfect gas relationship

$$\rho = \frac{P}{RT}$$

the uncertainty in the density can be related to the uncertainties in the measured pressure and temperature:

$$\frac{\delta \rho}{\rho} = \sqrt{\left(\frac{\delta P}{P}\right)^2 + \left(\frac{\delta T_b}{T_b}\right)^2}$$

Special consideration must be given to the wall shear stress uncertainty, particularly for local friction factors. The wall shear stress is given by

$$\tau_w = \frac{D}{4}\frac{d}{dx}\left[P + \frac{G^2}{\rho g_c}\right]$$

The uncertainty in the wall shear stress includes the uncertainties in P, G, ρ, and the operation of graphically determining the derivative. A reasonable estimate of the uncertainty interval, $\delta \tau_w$, which included these uncertainties, was made.

NUMERICAL EVALUATION OF UNCERTAINTY INTERVALS

The table on the following page contains a summary of the estimated uncertainties and the subsequent values of uncertainty interval in the calculated results, h and f; the necessary calculations were made as outlined above. The uncertainty intervals in the table are to be regarded as typical rather than specific values. It should be noted that the uncertainty presented for the local heat transfer coefficient is not valid in a region close to the lower electrode $\left(\frac{X}{D} < 10\right)$. There, the large axial conduction heat loss, with its high uncertainty, causes a greatly increased uncertainty in the heat transfer coefficient.

Summary of Uncertainty Analysis

Variable	Defined Uncertainty Interval	Estimated Uncertainty Interval
q'_T	$\frac{\delta q'_T}{q'_T - (q'_r + q'_a)}$	$\pm$ 2%
q'_r	$\frac{\delta q'_r}{q'_r}$	$\pm$ 5%
q'_a	$\frac{\delta q'_a}{q_a}$	$\pm$ 50%
w, G	$\frac{\delta w}{w} = \frac{\delta G}{G}$	$\pm$ 1%
T_w	$\delta T_w = \delta T_{wo}$; $\frac{\delta T_w}{T_w - T_{aw}}$	$\pm 5^{\circ}F$; $\pm$ 2%
$T_{b,e}$	$\delta T_{b,e}$; $\frac{\delta T_{b,e}}{T_{b,e}}$	$\pm 3^{\circ}F$; $\pm$ 0.6%
$T_{b,o}$	$\frac{\delta T_{b,o}}{T_{b,o}}$	$\pm$ 4.3%
T_{aw}	$\frac{\delta T_{aw}}{T_{aw}} = \frac{\delta T_{b,o}}{T_{b,o}}$; $\frac{\delta T_{aw}}{T_w - T_{aw}}$	$\pm$ 4.3% ; $\pm$ 8.6% *
P	$\frac{\delta P}{P}$	$\pm$ 2%
ΔP	$\delta(\Delta P)$; $\frac{\delta(\Delta P)}{\Delta P}$	$\pm .025_{psi}$; $\pm$ 0.5%

*Calculated Values

$\overline{q'_w}$	$\frac{\delta \overline{q'_w}}{\overline{q'_w}}$	$\pm$ 3.4% *
q''_w	$\frac{\delta q''_w}{q''_w}$	$\pm$ 3.4% *
h	$\frac{\delta h}{h}$	$\pm$ 9.5% *
ρ	$\frac{\delta \rho}{\rho}$	$\pm$ 4.8% *
τ_w	$\frac{\delta \tau_w}{\tau_w}$	$\pm$ 11%
f	$\frac{\delta f}{f}$	$\pm$ 12% *

*Calculated Values

APPENDIX E. PROPERTIES OF NITROGEN

The major reference for the properties used in this report is NBS circular 564 by Hilsenrath, et al. (9), a critical summary of gas property data reported as of the year 1954. This source has been supplemented by more recent work, primarily the thermal conductivity measurements of Vines (21).

1. Enthalpy

Hilsenrath, et al., calculated enthalpy over the range of temperatures and pressures needed for this report. Their values appear to be as accurate as any now available and are in excellent agreement with those recently calculated at the Franklin Institute (19).

2. Viscosity

The calculations of Hilsenrath, et al., are based on the Leonard-Jones 6-12 model of kinetic theory and fit the available experimental data, reported at temperatures as high as 2300°F, within ± 2 per cent.

3. Thermal Conductivity

As of 1954, reliable experimental data for the thermal conductivity of nitrogen extended only to 890°F. Hilsenrath, et al., fit a semiempirical equation to this data and extrapolate to 1700°F. However, the extrapolation, in the range of 900-1650°F, relies heavily on the data of Stops (16), which are probably 3 1/2 per cent too low at 1650°F. The more recent investigations of Vines (21) and Timrot and Vargaftig (20) extend to 1650°F and are in good agreement. Their data, and the low temperature data, are well correlated by an equation proposed by F. G. Keyes and reported by Vines. This equation is plotted in Figure 13.

4. Prandtl Number

The Prandtl number has been calculated as $\mu C_p/k$ using the enclosed viscosity and thermal conductivity curves and values of specific heat taken from NBS circular 564.

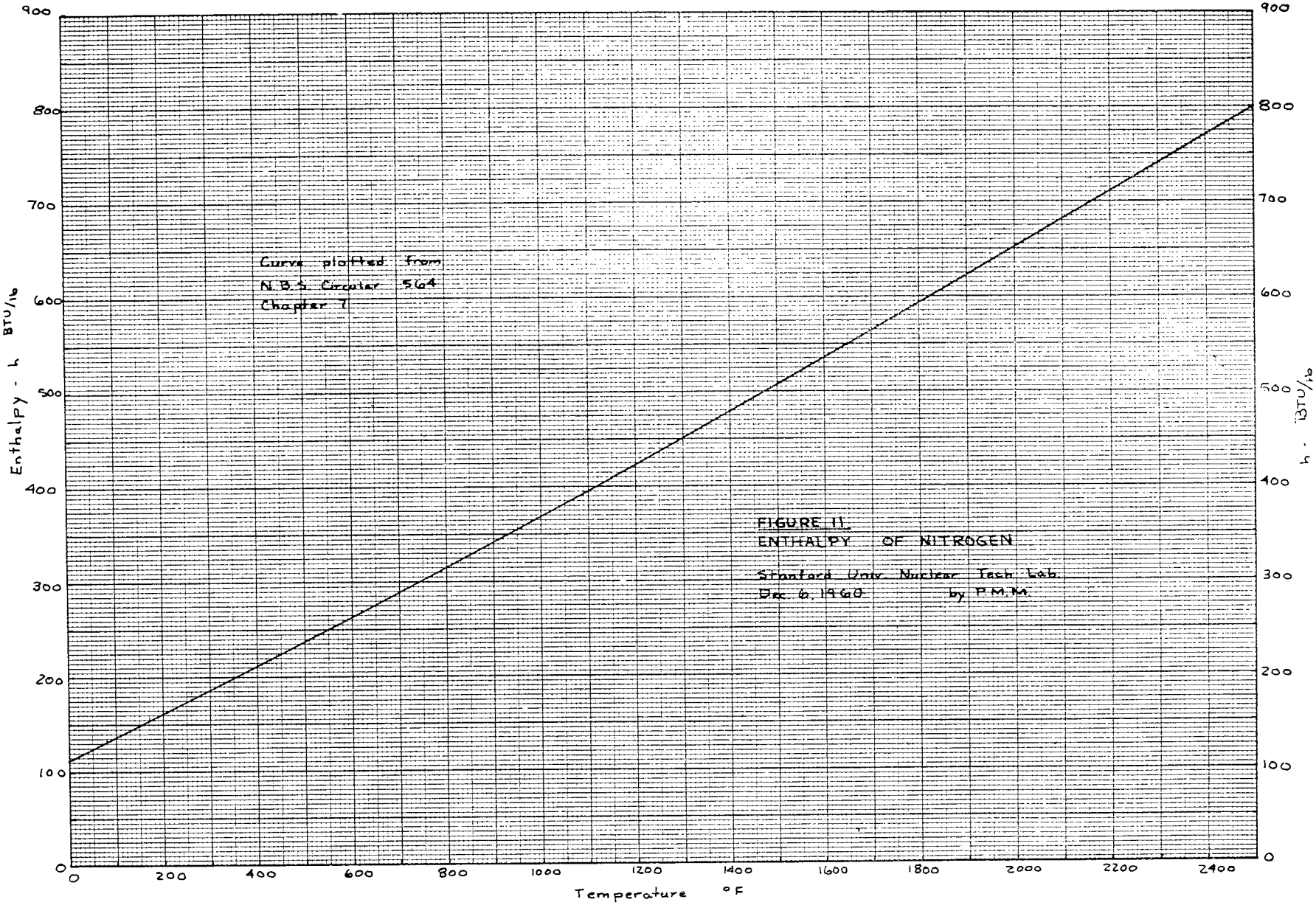

FIGURE 11
ENTHALPY OF NITROGEN

Stanford Univ. Nuclear Tech. Lab.
Dec 6, 1960 by P.M.M.

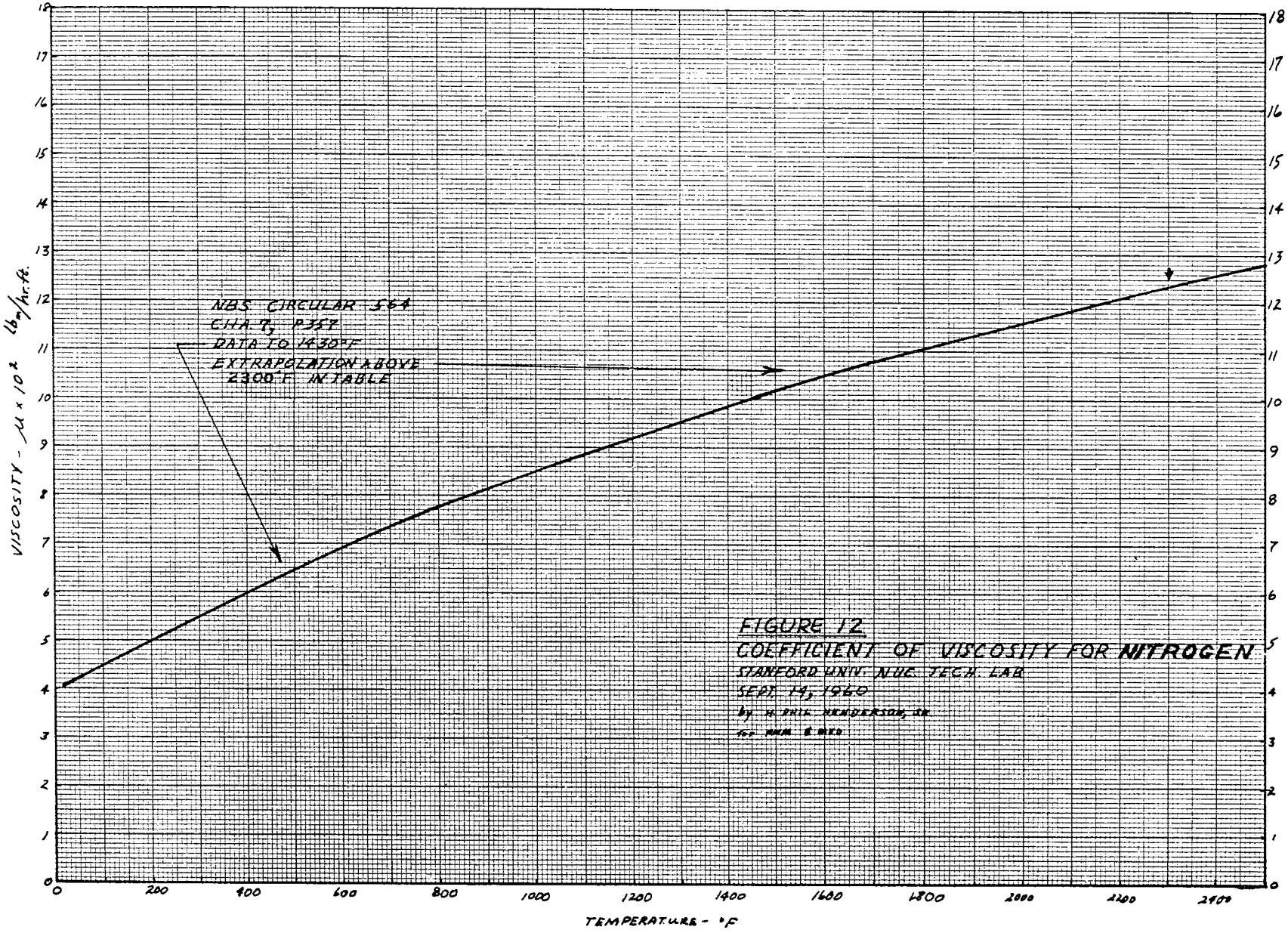

FIGURE 12
COEFFICIENT OF VISCOSITY FOR NITROGEN
STANFORD UNIV. NUC. TECH. LAB.
SEPT. 14, 1960
by H. ERIC HENDERSON JR.
ICC MMM & MED

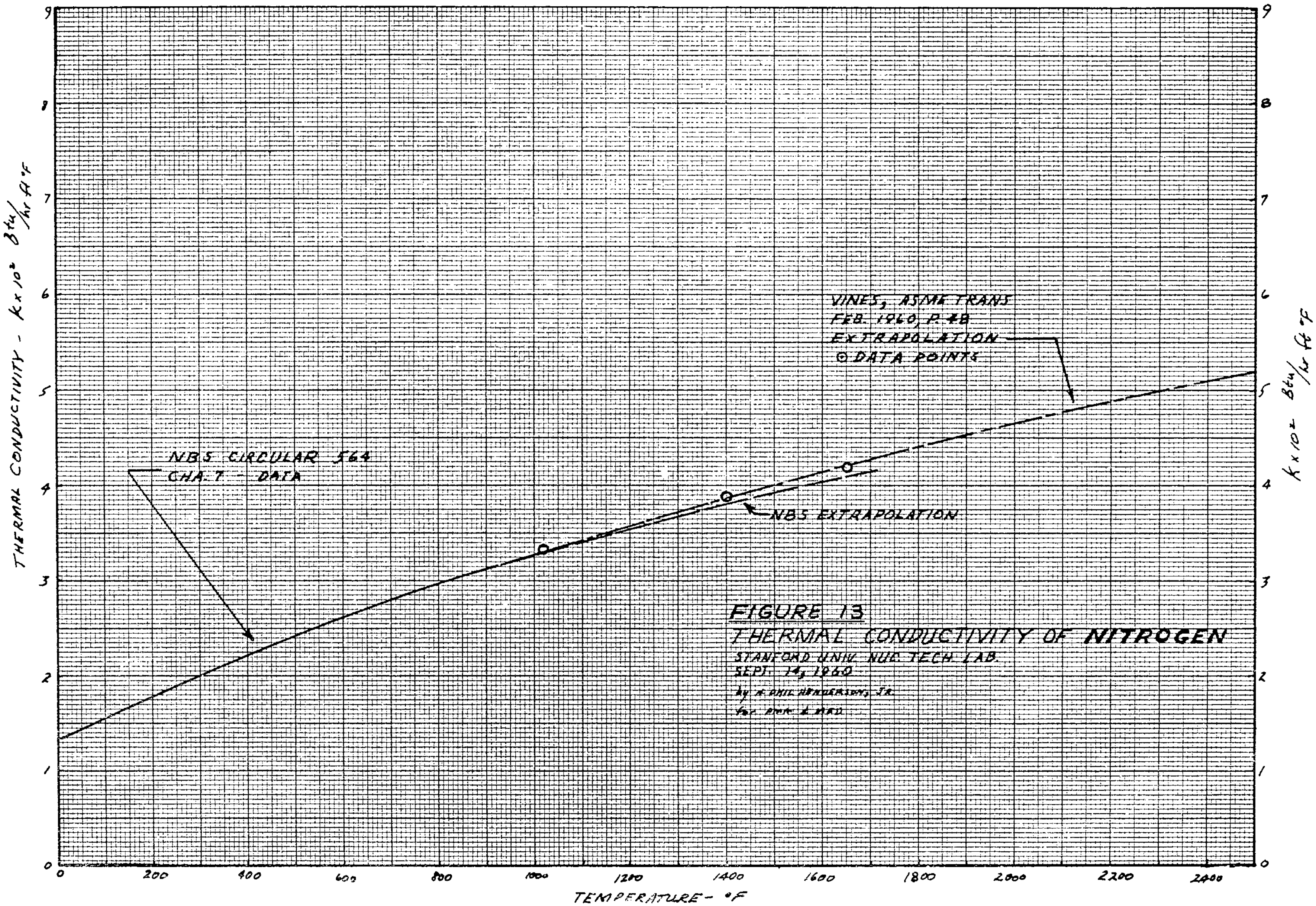

FIGURE 13
THERMAL CONDUCTIVITY OF **NITROGEN**
STANFORD UNIV. NUC. TECH. LAB.
SEPT. 14, 1960
by A. PHIL HENDERSON, JR.
for PHR & HRD

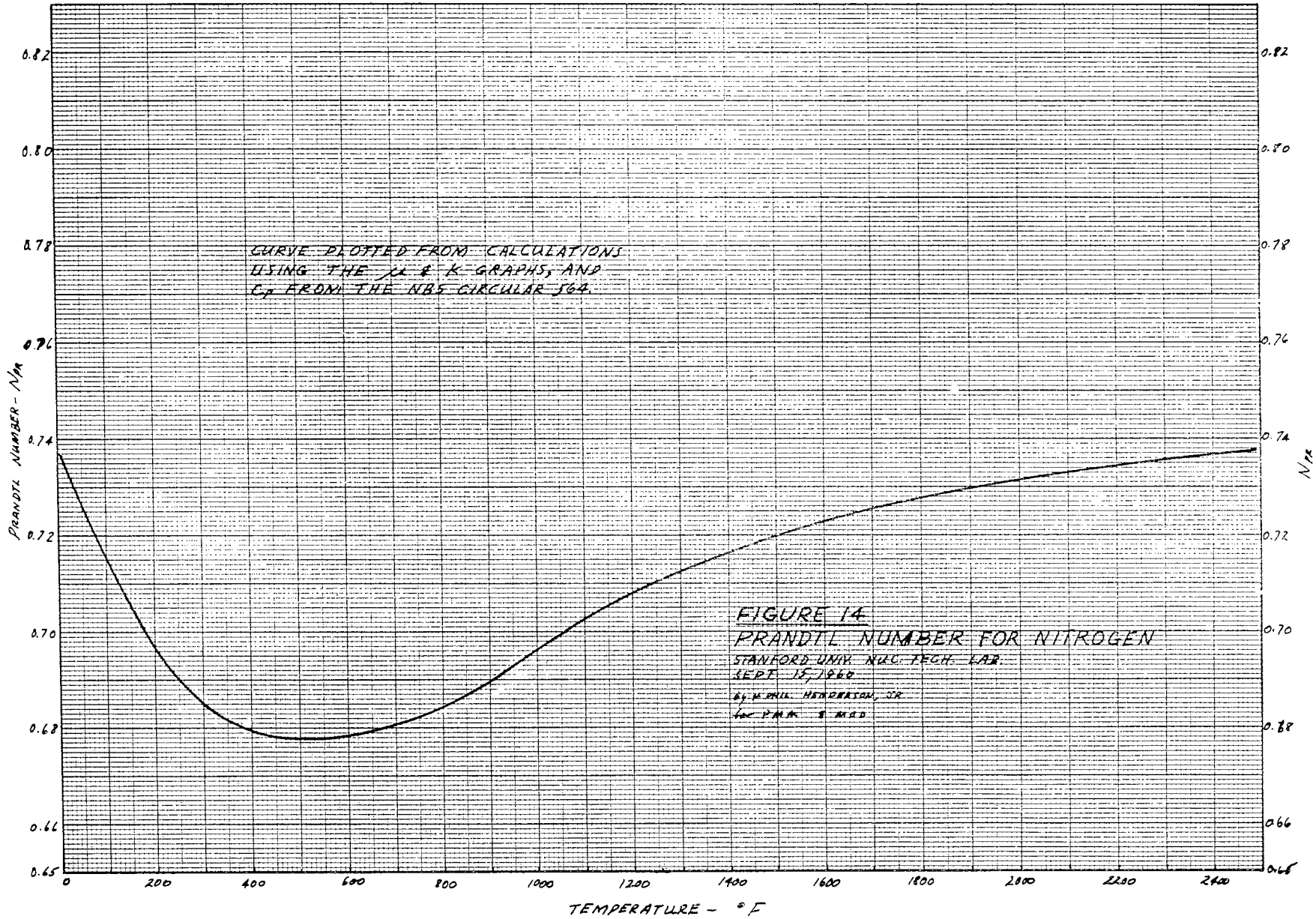

FIGURE 14
PRANDTL NUMBER FOR NITROGEN
STANFORD UNIV. NUC. TECH. LAB.
SEPT. 15, 1960
BY W. PAUL HENDERSON, JR.
for P.M.R. & M.E.D.

APPENDIX F. 4000°F EXPERIMENTAL APPARATUS

A new test section assembly and pressure vessel have been designed and constructed to measure local and average convective heat transfer coefficients for helium flowing through round tubes with gas temperatures as high as 4000°F. The new components are compatible with the present test apparatus and can be used interchangeably with the 2500°F test section assembly and pressure vessel. Figure 15 shows the new pressure vessel prior to welding, and Figure 16 is a schematic drawing of the test section.

The pressure vessel is formed from a 33-inch length of 5 inch diameter, scheduled 80 steel pipe, cut parallel to its axis to provide a four inch wide side opening. The pipe is welded onto a rectangular flange and is closed on the ends by two arc-shaped pieces. A one-inch thick, flat, steel plate bolts to the flange, the pressure seal being made with a copper gasket. A row of six view ports are located on the cover plate so that a radiation pyrometer can sight on the test section tube inside the pressure vessel. The viewing windows are 3/4-inch diameter quartz glass cylinders, each 3/4-inch long.

Pressure tap and thermocouple packing gland fittings are provided on the vessel's side. Electrode packing glands are located on the two ends of the vessel, as are fittings for the entrance and exit of the test gas.

Helium enters through the lower end of the pressure vessel into a mixing chamber where the bulk average temperature of the gas is measured with a chromel-alumel thermocouple probe. The gas then enters the test section, a 1/8-inch diameter thin-walled tantalum tube with a heated length of 20 inches. An unheated entrance length of four inches is provided to insure that the gas velocity profile is fully developed by the initial point of heating. After it has flowed through the test section, the helium is allowed to escape into the enclosing pressure vessel, thus equalizing the pressures on the inside and outside of the test section tube.

The test section tube is resistively heated by passing an electric current through it. Current is carried to the test section through a rigid inconel electrode clamped onto a tapered nickel plug, which, in turn, is brazed to the tube near the lower end, and through a graphite plug to a tantalum electrode at the upper end of the test section. The center of the

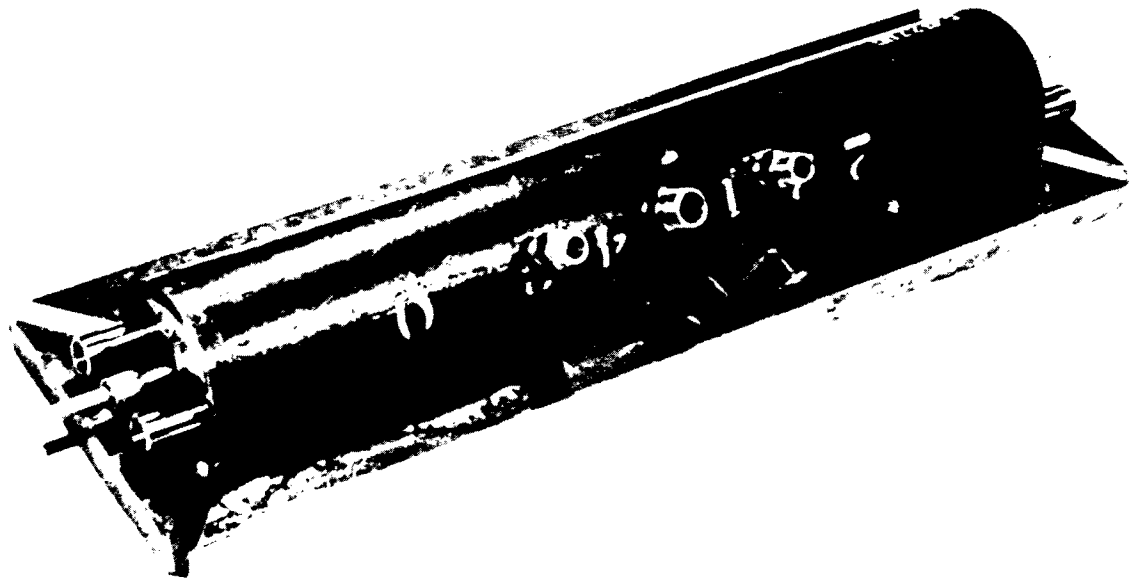

Figure 15 Pressure Vessel, 4000 °F Test Section

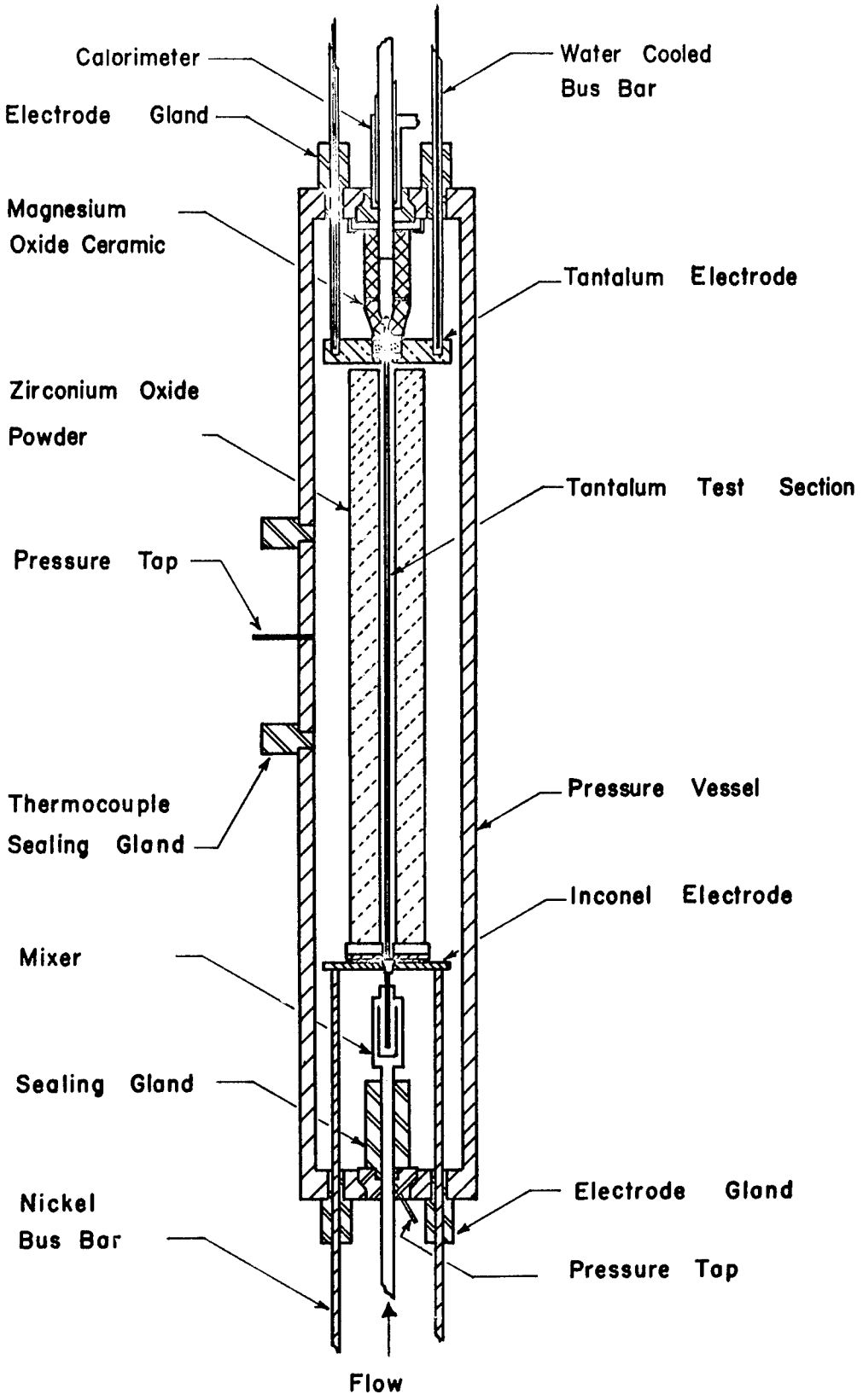

Figure 16 4000°F Test Section Assembly

tantalum electrode is filled with graphite powder compressed between two graphite retaining rings.

Pressure, applied to the upper retaining ring by means of a tension-loaded magnesium piece, insures good electrical contact. Since the graphite offers little resistance to slip, the tantalum test section is free to undergo thermal expansion.

Insulation of the test section is provided by two materials: fully stabilized zirconium oxide powder in regions of high temperature and micro-quartz fibrous insulation at lower temperature. The zirconium oxide powder is packed into an annulus formed by a 1/2-inch diameter tantalum tube, which also serves as a radiation shield, and a 2.5 inch diameter inconel tube. Micro-quartz insulation fills the remainder of the pressure vessel. The insulation reduces the radial heat loss from the test section to about 10 per cent of the total power input and limits the maximum temperature of the pressure vessel walls.

The outside wall temperature of the heated test section is measured at six axial locations by a radiation pyrometer sighting through the view windows provided on the pressure vessel. Small tantalum tubes pass through the insulation to give a clear view of the test section. In addition, wall temperatures are also measured with platinum-platinum-rhodium thermocouples welded to the test section. These thermocouples are limited to temperatures below 3100°F, but they provide a valuable check on the pyrometer readings at these temperatures.

The helium leaves the pressure vessel through a water-jacketed inconel tube which forms the first section of a calorimeter. The calorimeter cools the exhaust gas to a temperature that can be measured by a chromel-alumel thermocouple placed in a mixing chamber. Additional measurements of the gas and water flow rates, and of the entering and leaving water temperatures, allow the bulk temperature of the gas leaving the test section to be calculated. A second cooling section is installed in the exhaust line as the helium is still too hot after passing through the calorimeter to flow immediately through the exhaust valve.

LIST OF REFERENCES

1. Barnes, J. F., "An Experimental Investigation of Heat Transfer from the Inside Surface of a Hot Smooth Tube to Air, Helium and Carbon Dioxide," Report No. R. 241, National Gas Turbine Establishment, Pyestock, Hants (Great Britain), March 1960.

2. Davenport, Monty E., and Patrick M. Magee, "Heat Transfer to a Gas at High Temperature," Tech. Report No. 247-1, Nuclear Technology Laboratory, Stanford University, May 1960.

3. Deissler, R. G., "Heat Transfer and Fluid Friction for Fully Developed Turbulent Flow of Air and Supercritical Water with Variable Fluid Properties," Transactions ASME, vol. 76, 1954, pp. 73-85.

4. Deissler, R. G., "Analysis of Turbulent Heat Transfer, Mass Transfer, and Friction in Smooth Tubes at High Prandtl and Schmidt Numbers," NACA Report 1210, 1955.

5. Deissler, R. G., "Analytical Investigation of Turbulent Flow in Smooth Tubes with Heat Transfer with Variable Fluid Properties for Prandtl Number of 1," NACA Technical Note 2242, December 1950.

6. Deissler, R. G., and C. S. Eian, "Analytical and Experimental Investigation of Fully Developed Turbulent Flow of Air in a Smooth Tube with Heat Transfer with Variable Fluid Properties," NACA Technical Note 2629, February 1952.

7. Durham, F. P., R. C. Neal and H. J. Newman, "High Temperature Heat Transfer to a Gas Flowing in Heat Generating Tubes with High Heat Flux," Reactor Heat Transfer Conference sponsored by the U.S. Atomic Energy Commission, New York, November 1 and 2, 1956.

8. Eckert, E.R.G., and Robert M. Drake, Jr., Heat and Mass Transfer, second edition, McGraw-Hill Book Company, Inc., New York, 1959.

9. Hilsenrath, Joseph, Charles W. Beckett, William S. Benedict, Lilla Fano, Harold J. Hoge, Joseph F. Masi, Ralph L. Nuttall, Yeram S. Touloukian, and Harold W. Woolley, Tables of Thermal Properties of Gases, National Bureau of Standards Circular 564, November 1, 1955.

10. Humble, Leroy V., Warren H. Lowdermilk and Leland G. Desmon, "Measurements of Average Heat-Transfer and Friction Coefficients for Subsonic Flow of Air in Smooth Tubes at High Surface and Fluid Temperatures," NACA Report 1020, 1951.

11. Kline, S. J. and F. A. McClintock, "Describing Uncertainties in Single-Sample Experiments," Mechanical Engineering, January 1953.

12. Lapides, M. E., and M. B. Goldstein, "Heat Transfer Source File Data," APEX 425, General Electric Aircraft Nuclear Propulsion Department, Cincinnati 15, Ohio, November 1958.

13. McAdams, William H., Heat Transmission, 3rd Edition, McGraw-Hill Book Company, Inc., New York, 1954.

14. Nicoll, W. B. and W. M. Kays, "The Influence of Temperature Dependent Properties on Gas Flow Heat Transfer in Circular Tubes," Technical Report No. 43 prepared under contract Nonr 225(23) (NR-090-342) for Office of Naval Research, Stanford University, Stanford, California, September 1, 1959.

15. Shapiro, Ascher H., The Dynamics and Thermodynamics of Compressible Fluid Flow, vols. 1 & 2, Ronald Press Company, New York, 1953.

16. Stops, D. W., "Effect of Temperature upon the Thermal Conductivity of Gases," Nature, vol. 164, 1949, p. 966.

17. Sze, B. C., "The Effect of Temperature-Dependent Fluid Properties on Heat Transfer and Flow Friction for Gas Flow," Ph.D. Dissertation, Department of Mechanical Engineering, Stanford University, Stanford, California, 1957.

18. Taylor, Maynard F. and Thomas A. Kirchgessner, "Measurements of Heat Transfer and Friction Coefficients for Helium Flowing in a Tube at Surface Temperatures up to 5900°R," NASA Technical Note D-133, October 1959.

19. "Thermodynamic Properties of Helium and Molecular Nitrogen," preliminary draft of tables prepared by the Franklin Institute for the U.S. Atomic Energy Commission, 1960.

20. Timrot, D. L., and N. B. Vargaftig, "Heat Conductivity, Viscosity, and Thermodynamical Properties of Steam at High Temperatures and Pressures," Transactions of Fourth World Power Conference, III, Lund-Humphries, London, 1952, p. 1642.

21. Vines, R. G., "Measurement of the Thermal Conductivities of Gases at High Temperatures," Transactions ASME, "Journal of Heat Transfer," February 1960, pp. 48-52.

22. Weiland, Walter F., and Warren H. Lowdermilk, "Measurements of Heat Transfer and Friction Coefficients for Air Flowing in a Tube of Length-Diameter Ratio of 15 at High Surface Temperatures," NACA Research Memo E53E04, July 9, 1953.

23. Wolf, Helmut, "Heating and Cooling Air and Carbon Dioxide in the Thermal Entrance Region of a Circular Duct with Large Gas to Wall Temperature Differences," Transactions ASME, "Journal of Heat Transfer," November 1959, pp. 267-279.